



VICTORIA UNIVERSITY
MELBOURNE AUSTRALIA

Effectiveness of green and cool roofs in mitigating urban heat island effects during a heatwave event in the city of Melbourne in southeast Australia

This is the Draft version of the following publication

Imran, Hosen M, Kala, J, Ng, A. W. M and Muthukumar, Shobha (2018)
Effectiveness of green and cool roofs in mitigating urban heat island effects during a heatwave event in the city of Melbourne in southeast Australia.
Journal of Cleaner Production, 197 (1). 393 - 405. ISSN 0959-6526

The publisher's official version can be found at
<https://www.sciencedirect.com/science/article/pii/S0959652618318298>
Note that access to this version may require subscription.

Downloaded from VU Research Repository <https://vuir.vu.edu.au/37719/>

Effectiveness of green and cool roofs in mitigating urban heat island effects during a heatwave event in the city of Melbourne in southeast Australia

H. M. Imran^{1,3}, J. Kala², A. W. M. Ng^{1,3}, and S. Muthukumaran^{1,3}

¹College of Engineering and Science, Victoria University, Melbourne, Australia

²Environmental and Conservation Sciences, School of Veterinary and Life Sciences, Murdoch University, Perth, Western Australia

³Institute for Sustainable Industries & Livable Cities, Victoria University, Melbourne, Australia

Abstract

This study evaluates the effectiveness of green and cool roofs as potential Urban Heat Island (UHI) mitigation strategies, and the impacts of these strategies on human thermal comfort during one of the most extreme heatwave events (27th - 30th January 2009) in the city of Melbourne in southeast Australia. The Weather Research and Forecasting model coupled with the Single Layer Urban Canopy Model including different physical parameterization for various types of roofs (conventional, green and cool roofs) is used to investigate the impacts of green and cool roofs. Results show that the maximum roof surface UHI is reduced during the day by 1°C to 3.8°C by increasing green roof fractions from 30% to 90%, and by 2.2°C to 5.2°C by increasing the albedo of cool roofs from 0.50 to 0.85. Cool roofs are more efficient than the green roofs in reducing the UHI with maximum differences of up to 1.4°C. The reductions of the UHI vary linearly with the increasing green roof fractions, but slightly non-linearly with the increasing albedo of cool roofs. The maximum reductions in wind speed are 1.25 m s⁻¹ and 1.75 m s⁻¹ with 90% green and cool roofs (albedo 0.85) respectively. While previous studies report that the advection of moist air from rural areas is a key mechanism, this study shows that this is not the case for the extreme heatwave event due to the very dry and warm conditions, and instead, convective rolls play a more important role. This study also shows that initial soil moisture for green roofs does not have a substantial impact on the UHI. Finally, green roofs improve human thermal comfort by reducing the Universal Thermal Comfort Index by up to 1.5°C and 5.7°C for pedestrian and roof surface levels respectively, and by 2.4°C and 8°C for cool roofs for the same levels.

Keywords: UHI mitigation, green & cool roofs, coupled WRF-SLUCM, Thermal Comfort, UTCI

1. Introduction

The increasing urban population is imposing a burden on the urban environment and climate. Urban dwellers are expected to contribute up to 70% of the world population by 2050 (O'malley et al 2014). Vegetated surfaces are continuously being converted into urban and

¹ Correspondence to: H.M. Imran, College of Engineering and Science, Victoria University, PO Box 14428, Melbourne, Victoria, Australia.
Phone: +61399195041
Fax: +61399194139
E-mail: ihosen83@gmail.com

built surfaces to meet the increasing demand of the increasing urban population. This increased urbanization has substantial impacts by altering the surface energy balance, and consequently, affects the regional hydro-climatology (Song and Wang 2015). One of the well-known urbanization effects on urban climate is the Urban Heat Island (UHI), which results in higher temperatures in urban areas as compared to surrounding non-urban and nearby rural areas. Primarily, the UHI occurs due to human modifications of surface properties by using construction materials with lower albedos and higher specific heat capacity (e.g., bitumen on roads), reductions in vegetated areas, the emission of anthropogenic heat (e.g., via air conditioning). In addition, anthropogenic climate change is expected to result in more frequent incidents of climate extremes such as heatwaves in several parts of the globe (e.g., Cowan et al 2014), and this poses additional threats to the urban environment (Field et al 2014).

The definition of heatwave can be different according to different sectors. This paper refers to the meteorological definition which is based on percentiles (Perkins and Alexander, 2013), as at least three consecutive days during which the average of maximum and minimum temperatures exceeds the climatological 95th percentile (Nairn and Fawcett, 2013). The UHI in combination with heatwave events severely affects human thermal comfort (HTC), ecosystems, the urban environment and the urban climate. The combination of UHI effects and heatwaves is becoming a very important issue in southeast Australia because of its hot summer season, with data from the Australian Bureau of Meteorology Melbourne regional office weather station showing that maximum temperatures reached up to 45.1°C and 43.9°C in January 2009 and 2014 respectively (Victorian Auditor General's Report 2014). Australia is also expected to experience an overall increase in the duration, frequency, and intensity of heatwaves under future climate change (Cowan *et al* 2014). Therefore, there is an urgent need to develop effective policies to make cities more resilient to anthropogenic impacts, such as heatwaves and the UHI.

Research on the mitigation of UHI effect has gained significant attention in recent years. A number of mitigation strategies in urban areas have been proposed in the literature, such as using more reflective construction materials (Morini et al 2017, Morini et al 2016, Touchaei et al 2016), geometry of buildings (e.g., orientation, shape) (Guan et al 2014), increasing urban vegetation fractions, and the use of green and cool roofs (Razzaghmanesh et al 2016, Razzaghmanesh and Razzaghmanesh 2017, Sharma et al 2016, Li et al 2014, Akbari et al 2003). All these studies show that increasing the proportion of green spaces and higher albedo materials in urban areas have potential in mitigating UHI effects in cities. According to Akbari *et al* (2003), green and cool roofs are effective strategies for mitigating UHI effects because of the substantial area covered by rooftops within cities. Both green and cool roofs reduce the UHI effects by reducing sensible heat flux, but the mechanism is different. Green roofs reduce sensible heat flux by providing shade and repartitioning available energy to increased latent heat flux via evapotranspiration. On the other hand, cool roofs reflect more incoming solar radiation due to higher albedo, and consequently, reduce sensible heat flux as a result of lower net radiation.

The effectiveness of green and cool roofs in mitigating UHI effects has been investigated based on different modeling techniques including building energy consumption (Rosenfeld *et al* 1998, Wong *et al* 2003) and hydrological budget (Carson *et al* 2013, Sun *et al* 2014) at different spatial scales. Several studies use regional climate models (RCMs) for investigating the effects of green and cool roofs on the urban environment at the synoptic scale (e.g., Synnefa *et al* 2008, Millstein and Menon 2011). In recent years, some studies have investigated the cooling effect of cool roofs by altering the albedo of urban areas by using RCMs (Morini *et al* 2017, Morini *et al* 2016, Touchaei *et al* 2016, Taha 2008a, Taha 2008b) and global climate models (GCMs) (e.g., Oleson *et al* 2010, Irvine *et al* 2011, Akbari *et al* 2012). The relatively coarse resolution of GCMs does not allow for an accurate representation of landscape heterogeneity, and hence, the complex physical processes in the urban canopy cannot be resolved. RCMs, on the other hand, are useful tools in assessing the effectiveness of green and cool roofs in mitigating the UHI, as they are able to better resolve cities by using urban canopy parameterizations which include sub-grid scale effects.

Smith and Roebber (2011) used the Weather Research and Forecasting (WRF) model (Skamarock *et al* 2005) coupled with single Urban Canopy Model (SLUCM) (Kusaka and Kimura 2004), referred to as WRF-SLUCM, to investigate the effects of green and cool roofs on the urban climate of the city of Chicago in the US. They did not consider direct parameterizations for green roofs but adjusted the albedo for the entire urban domain neglecting the physical processes (e.g., additional moisture added by green roofs) relevant to green roofs. A more comprehensive study including direct parameterizations of green and cool roofs has been conducted by Li *et al* (2014) over the Baltimore–Washington DC metropolitan region in the USA during a heatwave event. They introduced a new urban parameterization model, the Princeton UCM (PUCM) coupled to the WRF model to assess changes in surface and near surface UHI and showed that soil moisture plays an important role in improving the performance of green roofs by controlling evaporation efficiency, consistent with previous studies (Sun *et al* 2013). Several recent studies have assessed the effectiveness of green and cool roofs for UHI mitigation in city areas by using the coupled WRF-SLUCM model (Yang *et al* 2015, Sharma *et al* 2016). These latter have shown that green and cool roofs can substantially reduce roof surface temperature via a reduction in sensible heat flux. In addition, green and cool roofs alter the surface energy balance, which modifies the moisture and heat fluxes between the land surface and atmosphere, and weakens vertical mixing during the day, and hence, reduces the boundary-layer height (Miao *et al* 2009, Sharma *et al* 2016).

In Melbourne, and across southeast Australia, heatwaves have become more frequent in the last 20 years (Perkins-Kirkpatrick *et al* 2016). The city of Melbourne has experienced the two most severe heatwave events in 2009 and 2014 in the past 10 years and these events have contributed significantly to increased mortality. According to the Victorian Auditor General's Report (2014), these two heatwaves have caused 374 and 167 excess deaths respectively, in the state of Victoria. The average annual number of days above 35°C in the city of Melbourne is likely to double by 2030 and triple by 2070 (Climate Institute 2013). Additionally, the average intensity of heatwave has increased by 1.5°C with the peak

heatwave day likely to be 2°C warmer than the long-term heatwave average in the city of Melbourne (Steffen *et al* 2014). Hence, there is a critical need to investigate UHI mitigation strategies, such as the use of green and cool roofs, for the city of Melbourne during heatwave events. Therefore, the present study investigates the effectiveness of green and cool roofs in mitigating UHI effects and explores the physical mechanisms/processes associated with these mitigation strategies during the heatwave event.

The WRF-SLUCM modeling system is used to evaluate the effectiveness of green and cool roofs in mitigating UHI effects in the city of Melbourne. Additional experiments are carried out with different initial soil moisture for green roofs to investigate the role of evapotranspiration in reducing the UHI. Furthermore, the paper focuses on the changes in boundary-layer dynamics as well as the effectiveness of green and cool roofs in improving the HTC, since UHI effects are exacerbated during heatwaves which increase heat-related illness and mortality. The key factors involved in improving HTC in urban areas during heatwave conditions are explored.

2. Methodology

2.1 Case Study

This paper focuses on an extreme heatwave event lasting 3 days from the 27th to the 30th of January in 2009. This event was selected because it is one of the most severe heat waves in southeast Australia, which preceded the devastating Black Saturday bushfires in early February 2009 (Engel *et al* 2013). This event occurred after a period of prolonged drought which is reported to have contributed up to 1°C to 3°C to the heatwave event (Nicholls and Larsen 2011), and antecedent soil moisture conditions have been shown to play an important role (Kala *et al.* 2015).

2.2. WRF Configuration

This study uses the WRFv3.8.1 model, which is a non-hydrostatic RCM (Skamarock *et al* 2008), which has been widely used for urban meteorology studies (e.g., Li and Bou-Zeid 2014, Li *et al* 2014, Yang *et al* 2015, Sharma *et al* 2016). The model was operated with three nested domains (d01, d02, and d03) as illustrated in Figure 1(a) showing the three domains at 18 km, 6 km and 2 km resolution respectively. The second domain (d02) covers a large part of the state of Victoria while the innermost domain (d03) covers the Melbourne metropolitan area and surrounding rural areas. Following Imran *et al.* (2017), land-use categories from USGS were used to define the dominant land-use type for each grid cell. To obtain a more accurate representation of urban land-use, the global urban land-use dataset of Jackson *et al* (2010) was used to represent the variability of urban categories in the modeling domain. The Jackson *et al* (2010) data set represents four categories of urban areas (low-density urban, medium density urban, high-density urban and tall building areas) and properties such as urban morphology, urban extent, and radiative and thermal properties of building materials. In this study, we used the spatial extent of urban areas from Jackson *et al.* (2010) to re-classify all urban grid cells as either low-density urban, high-density urban, or commercial/industrial areas, as required by the SLUCM. The low and medium density urban

areas of the Jackson et al. (2010) land-use dataset were classified as low-density and high-density urban areas respectively, while the high-density urban areas and tall buildings were classified as commercial/industrial areas, as illustrated in Figure 1(b). Such a re-classification allowed for a realistic representation of urban land-use categories for the region. Finally, non-urban land use categories were modified based on the Australian Land Use and Management Classification Version 7 (<http://www.agriculture.gov.au/abares/aclump/land-use/alum-classification>). The dominant land use categories across the model domain are shown in Figure 1(b).

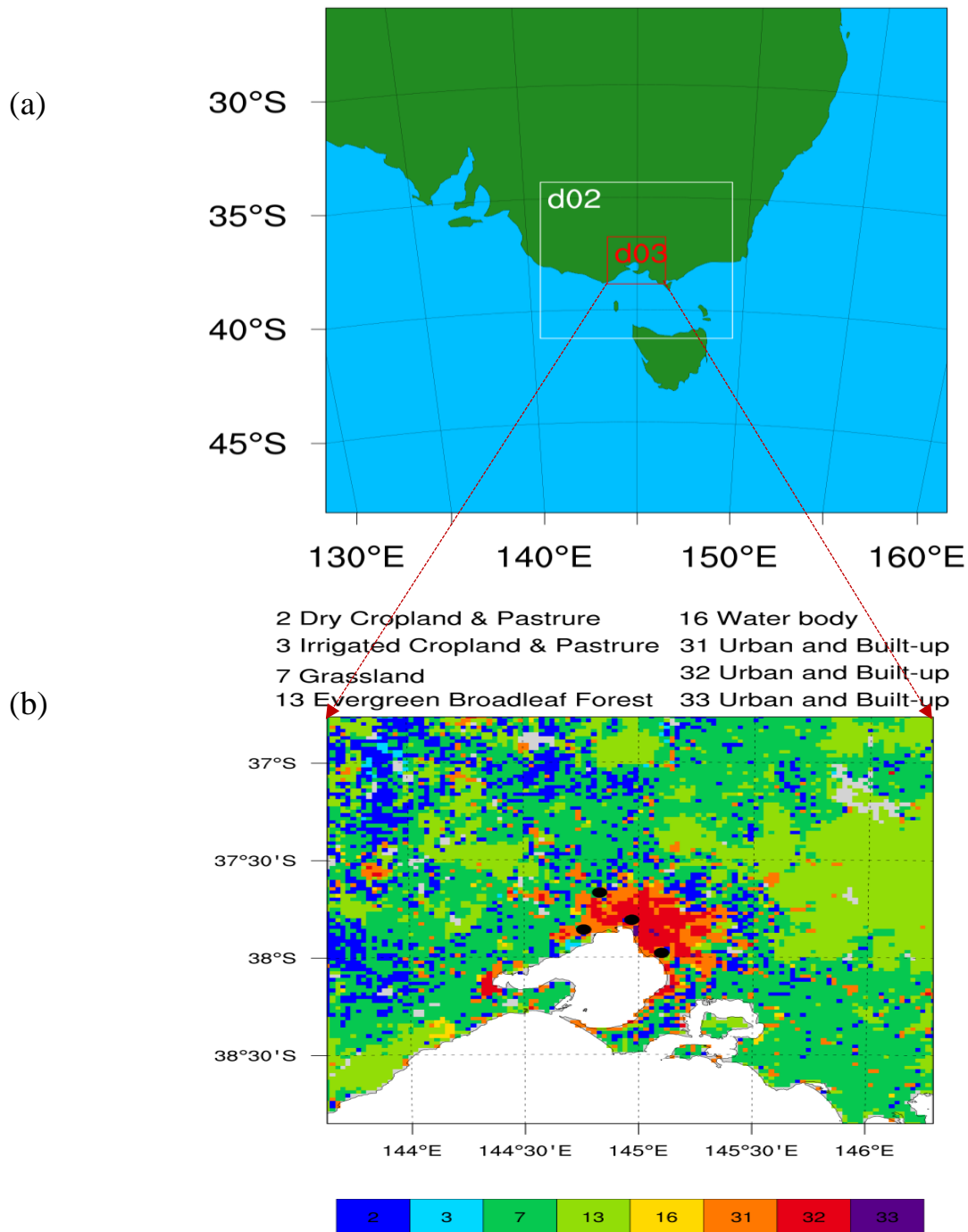


Figure 1. (a) WRF domain configuration, d02 represents the second domain which has a resolution of 6 km, and d03 represents the innermost domain with a resolution of 2 km. (b)

Dominant land use categories in the innermost domain (d03) with the locations of four weather stations (Black Circles) from the Australian Bureau of Meteorology, used for evaluation.

As part of configuring the WRF model, a user needs to specify the number of vertical atmospheric levels to be used. Following Imran et al. (2017), this study used 38 vertical levels from the surface to 50 hPa (top of the atmosphere), with levels more closely spaced close to the surface, so as to better resolve near surface atmospheric processes, and wider apart in the upper troposphere where high vertical resolution is not required. The WRF model offers multiple options for different physical parameterizations, including cloud microphysics (MP), planetary boundary layer (PBL), radiation, land surface model (LSM) and cumulus processes, and the model is well documented to be sensitive to the choice of physics options (e.g., Evans *et al* 2012, Kala *et al* 2015). The choice of physical parameterizations was based on Imran et al. (2017) who investigated the sensitivity of WRF to different physical parameterizations and provided an ideal set-up for the simulation of heatwaves in southeast Australia. This includes: (a) the Noah LSM (Chen and Dudhia 2001) coupled with the SLUCM (Chen and Dudhia 2001, Liu *et al* 2006, Chen *et al* 2011), (b) the Mellor–Yamada–Janjic (MYJ) PBL scheme (Janjić 1994), (c) the Thompson MP (Thompson *et al* 2008), (d) the RRTMG shortwave and longwave radiation schemes (Iacono *et al* 2008). No cumulus physics parameterization is used for the domain d03 as convection is resolved at 2 km resolution, while the Grell3D scheme (Grell and Dévényi 2002) is used for the outer two domains d01 and d02. The interactions between these different physical parameterizations is illustrated in Figure 2. For a more detailed description of the WRF model, we refer the reader to Skamarock et al. (2005), and for more details on WRF configuration, we refer the reader to WRF user’s guide available online at http://www2.mmm.ucar.edu/wrf/users/docs/user_guide_V3/contents.html. The initial and boundary conditions for the WRF simulations were obtained from 6-hourly ERA-interim reanalysis product with 0.75×0.75 degree spatial resolution available from 1970 onwards (Dee *et al* 2011). All analysis has been performed considering only the innermost domain (d03) for Melbourne metropolitan area.

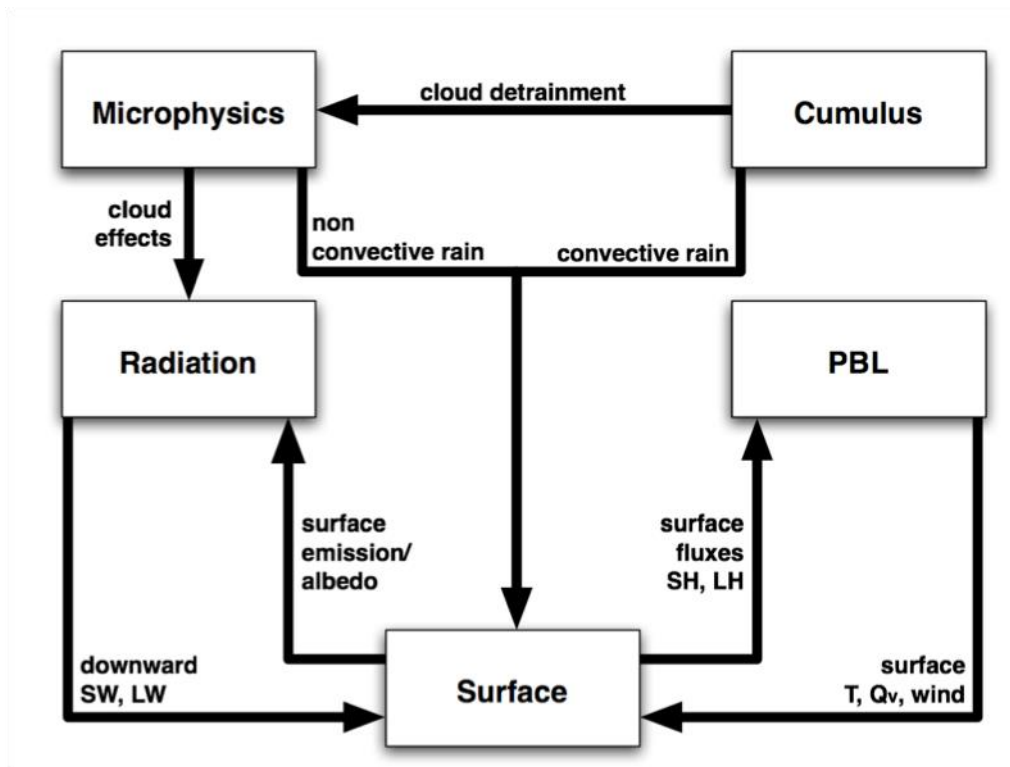


Figure 2. Interactions between different physical parameterizations in the WRF model (Dudhia 2014).

2.3. Numerical set-up of green and cool roofs

The updated SLUCM incorporates various urban parameterizations for green and cool roofs (Chen *et al* 2011). The SLUCM takes into consideration important properties of the urban canyon environment including solar azimuth angle, orientations of an urban canyon and the shadowing effects of buildings (Kusaka *et al* 2001). The model diagnoses air temperature, skin temperature, wind speed, relative humidity and fluxes from all surfaces within the canopy. The SLUCM resolves air temperature at the top of the canopy exchanged with the lowest level of the atmosphere incorporating all factors within the urban canopy (Smith and Roebber 2011).

Green roofs in the SLUCM consist of four different layers and a vegetation layer, and an urban irrigation algorithm is included. The total depth of the four layers is 50 cm including a 15 cm loam soil (5 cm top soil + 10 cm soil) layer for grassland, 15 cm growing medium layer, and 20 cm for concrete roof layer. In the SLUCM, the grid cells are treated as urban if the dominant land use category is classified as either low-density urban or high-density urban or commercial/industrial areas. When the SLUCM is used, an urban grid cell is further divided into an impervious and a grass-covered fractions as described by Chen *et al.* (2011). The grass fraction of the SLUCM represents urban parks and lawns and captures small scale variability inside the built terrain (Li *et al.* 2013). Figure 3 shows a typical schematic diagram for impervious and vegetated fractions in the SLUCM for different roofs. Urban/built fraction includes buildings, roads, pavements and artificial built surfaces while vegetated fraction

incorporates a cropland/grassland mosaic. The figure also illustrates energy fluxes for conventional, green and cool roofs.

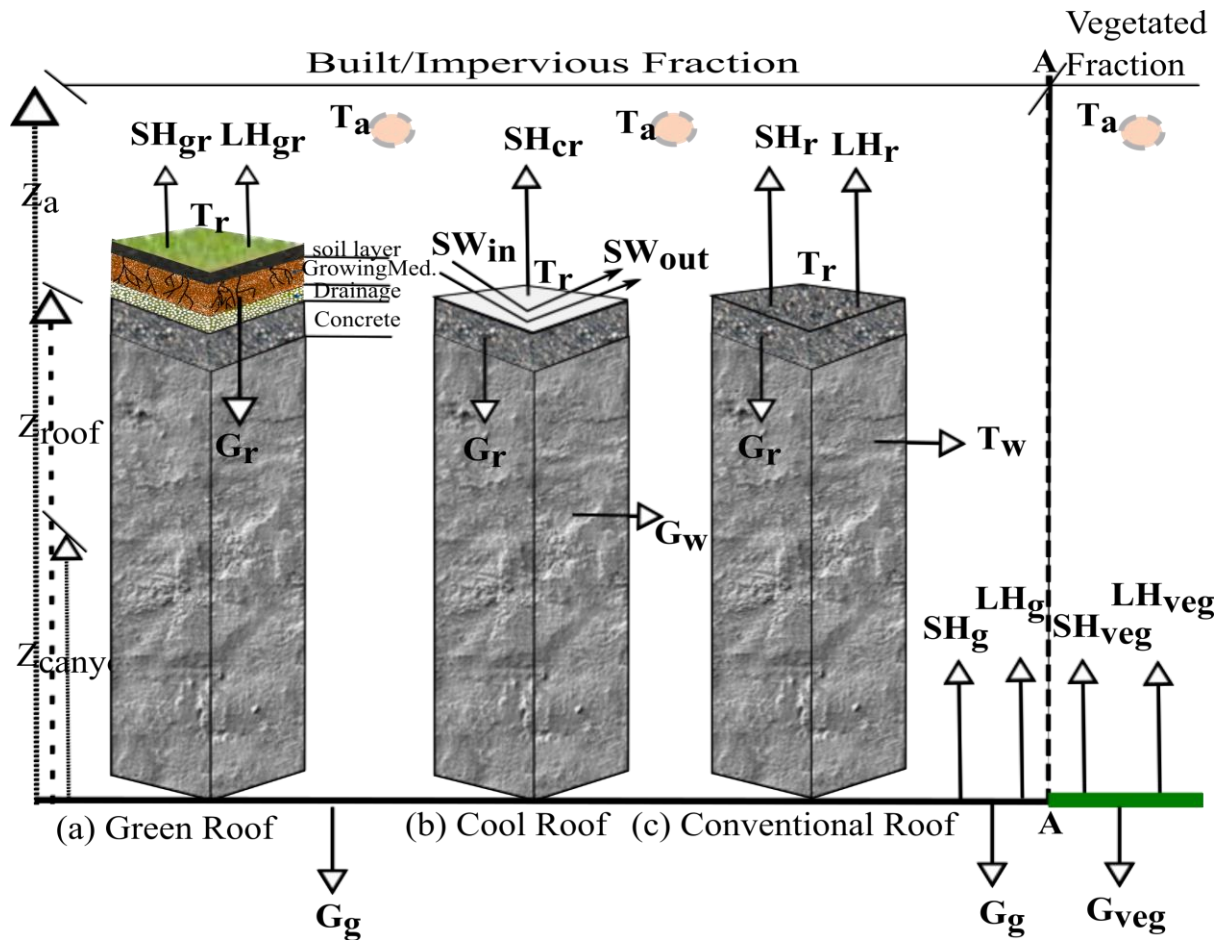


Figure 3. A typical framework of an urban grid cell in the WRF-SLUCM. The SLUCM incorporates a built/impervious fraction (left side of line A-A) and another vegetated fraction (right side of bold dotted line-A). The subscripts a, cr, g, gr, r, veg, and w represent air, cool roof, ground, green roof, conventional roof, vegetation and wall, respectively while the T, SH, LH, G and SW represent temperature, sensible heat flux, latent heat flux, storage heat and shortwave radiation. Finally, Z_{canyon} , Z_{roof} and Z_a represents street canyon height, rooftop height, and the first level of atmospheric model (adapted from Sharma *et al* 2016).

The urban morphological properties used in this study are the same as the properties used in the default WRF model, except for the built/impervious fraction for low-density urban areas (Table 1). The SLUCM includes several parameters for each of the three urban categories, and the default parameters may not necessarily be representative for a particular city. Although the default impervious fraction in the WRF model is 0.50 for the low-density urban area, this study uses a 0.70 impervious fraction for the same area based on previous study by Coutts *et al* (2007), who used urban fraction 0.71 for low-density areas for the city of Melbourne. Moreover, we found that the WRF model underestimated the near-surface temperature in our previous study (Imran *et al* 2017). Therefore, an urban fraction of 0.50 for low-density urban areas appears to be too low, and hence this study uses a fraction of 0.70 to obtain more realistic simulations as compared to observations. The use of a higher urban

fraction is also consistent with other studies whereby all urban areas were considered as high-density urban and assigned an urban fraction of 0.90 for all urban grid cells for the city of Sydney in Australia (Argueso et al 2014).

Table 1. The urban properties for the three urban categories used by the SLUCM.

Properties/Parameters	Low-Density Urban	High-Density Urban	Commercial/Industrial
Built/Impervious fraction	0.70 (default 0.50)	0.90	0.95
Roof width (Rf)	8.3 m	9.4 m	10 m
Road width (Rd)	8.3 m	9.4 m	10 m
Roof fraction in built/impervious part [Rf/(Rf + Rd)]	50 %	50 %	50 %
Roof fraction in whole urban grid	25 %	45 %	47.5 %
Building Height	5 m	7.5 m	10 m

2.4. Design of numerical experiments

Following Imran *et al* (2017), simulations are carried out from the 27th to the 30th of January 2009 with the first 24 hours considered as spin-up time and the remaining 72 hours are used for analyses. Hourly outputs are used to assess the effectiveness of green and cool roofs for mitigating the UHI effects. The numerical experimental set-up using different roofs is shown in Table 2. The effectiveness of green and cool roof strategies in mitigating UHI effects are investigated by running experiments with increasing green roof fractions and roof-top albedo of the urban grid cells. The first experiment is for the conventional roofs (control) with an albedo of 0.20. This numerical experiment is designed as a standard coupled WRF-SLUCM model by updating only three urban categories (low density, high density and commercial/industrial areas) according to the Jackson *et al* (2010) data-set for the city of Melbourne (Figure 1b). The non-urban grid cells were not modified. The second numerical experiments are carried out to examine the effectiveness of cool roofs by using different albedo values of 0.50, 0.70 and 0.85. The third series of experiments are conducted to evaluate the effectiveness of green roofs employing different percentages of green roof fractions of 30%, 50%, 70% and 90%. The choice of these percentages was based on a study by Sharma *et al* (2016) who showed that large percentages of green roof fractions are needed so as to result in noticeable effects of green roofs using the WRF-SLUCM. On the other hand, 100% cool roof is used for all cool roofs experiments as the default SLUCM does not have the functionality to alter the cool roof fraction, the idea being that the entire roof is painted or covered with reflective material. These reflective materials can be made of a highly reflective type of paint, a sheet covering, tiles or shingles. In the final numerical experiments, the cooling benefit of increased soil moisture in 50% green roofs is examined by using initial soil moisture of 0.30 and 0.40 m³ m⁻³ as compared to the default initial soil moisture of 0.15 m³ m⁻³ to examine the performance of green roofs under very dry conditions.

The default initial soil moisture of green roofs is $0.20 \text{ m}^3 \text{ m}^{-3}$. The rationale for using higher initial soil moisture was to investigate the effects of “once-off” irrigation at the start of the heat-wave event, and how long any subsequent cooling effects would last.

Table 2. Numerical experimental set-up

Numerical Experiment	Type of roof	Albedo	Cool Roof Fraction	Green Roof Fraction	Initial Soil Moisture
Control	Conventional	0.2	-	-	-
Cool	Cool	0.50, 0.70 and 0.85	100%	-	-
Green	Green	-	-	30%, 50% , 70% and 90%	-
SMOIS	Green	-	-	50%	0.15, 0.30 and $0.40 \text{ m}^3 \text{ m}^{-3}$

2.5. Outdoor HTC calculations

This study uses the UTCI index for representing the outdoor HTC by quantifying a physiological response based on meteorological input data. Although, there are several HTC indices such as the Discomfort Index, the approximate wet bulb globe temperature, and the Physiological Equivalent Temperature, for describing HTC, the UTCI is most widely used (Bröde *et al* 2012a, Vatani *et al* 2016).

The UTCI index is a widely accepted HTC index in representing bioclimatic conditions related to thermal stress under various climatic conditions which make this index more universal (Blazejczyk *et al* 2012). The RayMan Pro 3.1 model is used for calculating the UTCI where the default clothing factor of 0.9 and activity rate of 80 W is used for a male of 35 years age. The UTCI index considers not only air temperature effects on the human body but also other climatic factors of wind speed, relative humidity and solar radiation (Johansson 2006). The temperature, wind speed, relative humidity and solar radiation simulated by the WRF model are used as inputs in the RayMan model. The physical basis, abilities and limitations of RayMan have been discussed by Matzarakis *et al.* (2010). The UTCI index is classified into five categories as shown in Table 3 according to the scale proposed by Brode *et al.* (2012b).

Table 3. Universal Thermal Comfort Index (UTCI) range for different grades of human thermal perception and associated physiological stress (Bröde *et al* 2012b)

UTCI (°C)	Physiological Stress
+9 to +26	no thermal stress
+26 to +32	moderate heat stress
+32 to +38	strong heat stress
+38 to +46	very strong heat stress
> +46	extreme heat stress

3. Results and Discussion

3.1. Evaluation of the WRF Model

The WRF model has been evaluated for the Melbourne region in our previous study (Imran et al 2017), where we conducted an extensive sensitivity analysis of the WRF model to different physics options in simulating four heatwave events, including the case-study used in this paper. In our previous study (Imran et al 2017), we compared WRF simulations against station and gridded surface observations as well as atmospheric soundings. We tested a number of physics options for each physical parameterization and evaluated the WRF model based on statistical analyses. In addition, we carried out an in-depth analysis of the physical processes associated during heatwaves and how these physical dynamics were simulated by the model. Finally, we showed that the WRF model was able to simulate the various climate variables the city of Melbourne during heatwave events. As additional evaluation for this paper, we compare the simulated hourly near-surface temperature (T2) and wind speed (10 m) against observations from four weather stations in the urban region from the Australian Bureau of Meteorology (black circles in Fig 1(b)). The observed and simulated near-surface temperature and wind speed are averaged across the four weather stations. This is illustrated in Figure 4 showing that the simulated temperature and wind speed were very close to observations, with relatively small differences between the model and observations. The WRF simulations captured the observed near surface and wind speed reasonably well, although the model had a tendency to simulate the increase in wind-speed slightly earlier than observed. Together with our previous evaluation (Imran et al. 2017), Figure 4 shows that WRF performs satisfactorily and can be used for UHI studies, consistent with the existing literature (Sharma et al. 2014).

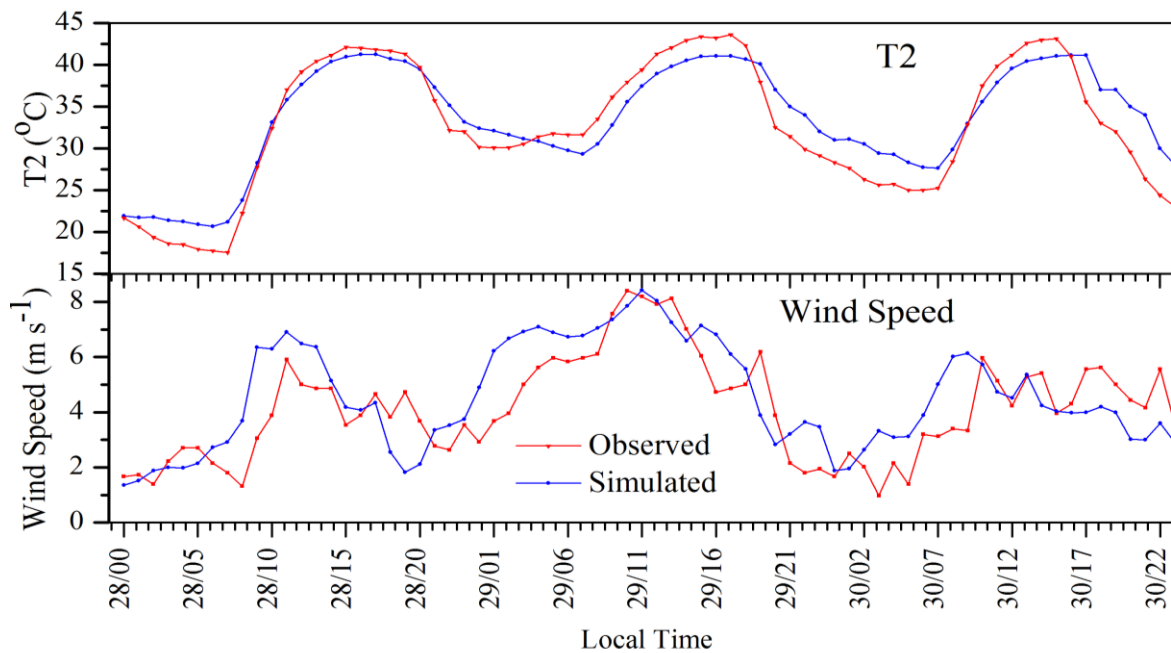


Figure 4. Comparison of observed and simulated near-surface temperature (top) and wind speed (bottom) for 28 – 30 January 2009 at four BoM weather stations (black circle in Figure 1(b)) in the urban areas. The mean from the four stations, and WRF outputs from the closest grid point to the stations are plotted.

3.2. Diurnal cycles of sensible heat flux and UHI

Diurnal cycles of sensible heat flux, near-surface, and roof surface UHI are shown in Figure 5 for the convective roof (control), cool roof (albedo 0.85), and 90% green roof experiments. The Control simulation shows that the city of Melbourne is experiencing a near-surface UHI from 1.5 to 5.7 °C, and a roof-surface UHI from 3.0 to 11.0 °C, and the maximum UHI occurs in the evening. Diurnal variations of simulated near-surface and roof-surface UHI have different hourly variations but reach their peak at the same time at 2000 local time while sensible heat flux reaches its peak at 1430 local time. The use of 90% green roof fraction results in lower sensible heat flux, near-surface and roof-surface UHI as compared to conventional roofs during the day while the cool roofs (albedo 0.85) result in the lowest sensible heat flux, near-surface and roof-surface UHI during both the day and night. The near-surface UHI shows an increasing trend during the day while the roof-surface UHI shows the opposite. Interestingly both green and cool roofs show maximum reductions during the day. Cool roofs with an albedo of 0.85 are more effective than 90% green roofs, with larger reductions in the sensible heat flux, near-surface and roof surface UHI. Although green roofs result in a slight warming during early morning, cool roofs substantially reduce warming effects during both the day and night. It is noteworthy that both green and cool roofs are also effective in reducing sensible heat flux, near-surface and roof surface UHI, even when they reach at their peaks.

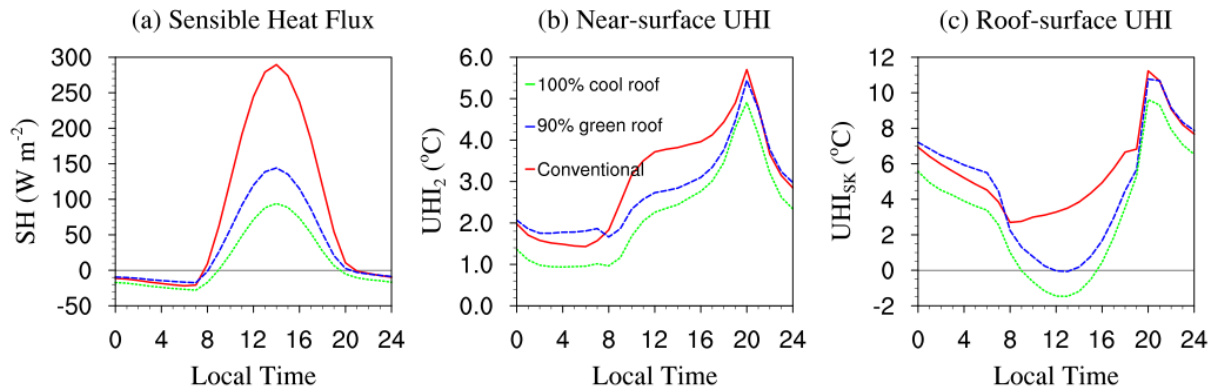


Figure 5. Diurnal variations of (a) sensible heat flux (W m^{-2}), (b) near-surface UHI (UHI_2) ($^{\circ}\text{C}$) and (c) roof surface UHI (UHI_{sk}) ($^{\circ}\text{C}$) from domain d03 averaged over 3 days (from 28th to 30th January 2009). Sensible heat flux results are averaged over urban grid points only and the UHI is the difference in near surface and roof surface temperature between urban and surrounding rural grid cells.

3.3. Effectiveness of green roofs in mitigating UHI effects

Figure 6 shows the energy balance of different green roof fractions in urban areas. Green roofs substantially reduce sensible heat flux, storage heat and net radiation, and increase latent heat flux. Increased green roof fractions (0% to 90%) can reduce the daily peak sensible heat flux by up to 150 W m^{-2} . Interestingly, green roofs especially 90% green roof fraction results in slightly higher sensible heat flux during the morning and late-night. The daily peak latent heat flux is higher by 70 W m^{-2} when 90% green roof fraction is used. The higher latent heat flux would be expected to result in larger reductions of roof surface temperature. This finding is reflected in in Figure 7 which shows that green roofs substantially reduce the roof surface UHI intensity during the day due to higher latent heat flux resulting from evapotranspiration. Although the differences in storage heat between green roof fractions and conventional roofs are small during early morning and late night, higher green roof fractions result in larger reductions of storage heat during the day. Usually, this energy is either stored into roofs and later released or conducted into the building indoor space and pumped back into the atmosphere by air conditioners (Li *et al* 2014). Green roofs have relatively lower positive values of storage heat flux being released back into atmosphere in the early morning and late night. On the other hand, green roofs show a higher reduction of storage heat being transferred to the buildings as compared to conventional roofs during the day. Net radiation is substantially reduced by the green roof fractions in the afternoon (1300 - 1800 local time). As reported by Sharma *et al* (2016), this is most likely due to slight increase in albedo by increasing green fractions.

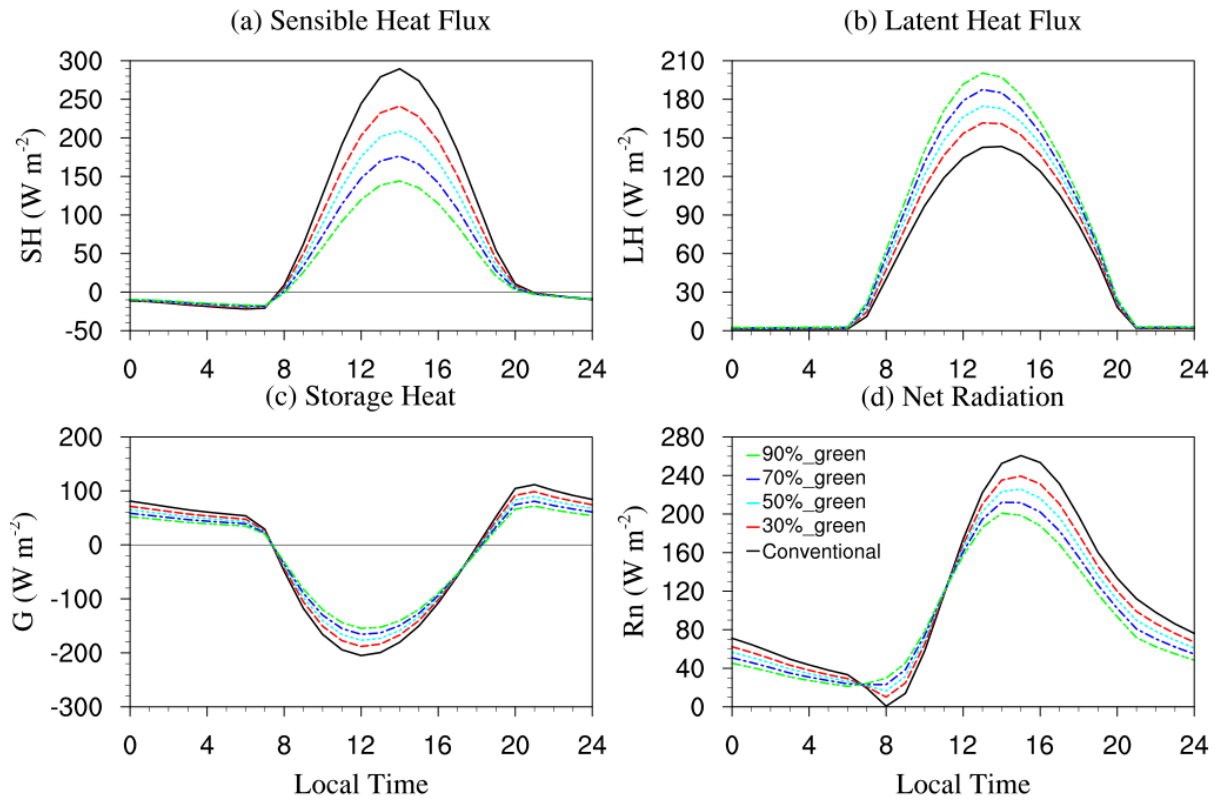


Figure 6. Diurnal variation of (a) sensible heat flux (b) latent heat flux, (c) storage heat, and (d) net radiation, averaged only over urban grid points in domain d03 over 3 days (from 28 – 30 January in 2009), for experiments with 30%, 50%, 70% and 90% green roof fractions and the control.

The city-scale effectiveness (i.e., considering all urban grid cells in the metropolitan areas) of different green roof fractions in reducing the UHI is shown in Figure 7 based on the ability of green roofs in reducing the maximum near-surface and roof surface UHI effects. The UHI is calculated as the difference between the urban and surrounding rural grid cells. The effectiveness of green roofs relative to conventional roofs in reducing the UHI is quantified as the difference of the UHI intensity between green roofs and conventional roofs ($\text{UHI}_{\text{green}} - \text{UHI}_{\text{conventional}}$). Figures 7(a) and 7(b) show the diurnal changes of the UHI at the near-surface and roof surface levels respectively while 7(c) and 7(d) illustrate the relationship between green roof fractions and the reductions of the UHI, averaged over three diurnal cycles from 28 – 30 January in 2009. The use of green roofs in urban areas has a substantial cooling effect across the whole metropolitan area due to a reduction in sensible heat flux. Increasing the green roof fractions from 0% to 90% results in maximum reductions of the near-surface UHI from 0.30 to 1.15°C and this occurs between 1200 and 1400 local time, while the maximum roof surface UHI reductions range from 1.0 to 3.8°C and this occurs between 1300 and 1500 local time. Interestingly, both the near-surface and roof surface UHI reductions vary linearly with increasing green roofs fractions (Figures 6(c) and 6(d)). The reductions of roof surface UHI are substantially higher (0.70 to 2.65°C) than the near-surface UHI during the day. This larger reduction of the roof surface UHI occurs due to higher evaporation and transpiration during photosynthesis during the day at the roof level. The lower reductions of the near-

surface UHI is likely due to radiation effects (trapping solar radiation between buildings) inside the canopy. The building facades, impervious surfaces and heights between green roof and ground surfaces plays important role on the dilution, dispersion and dissipation processes. On the other hand, the differences in near-surface UHI reductions among the green roof fractions are smaller than the reductions of the roof surface UHI.

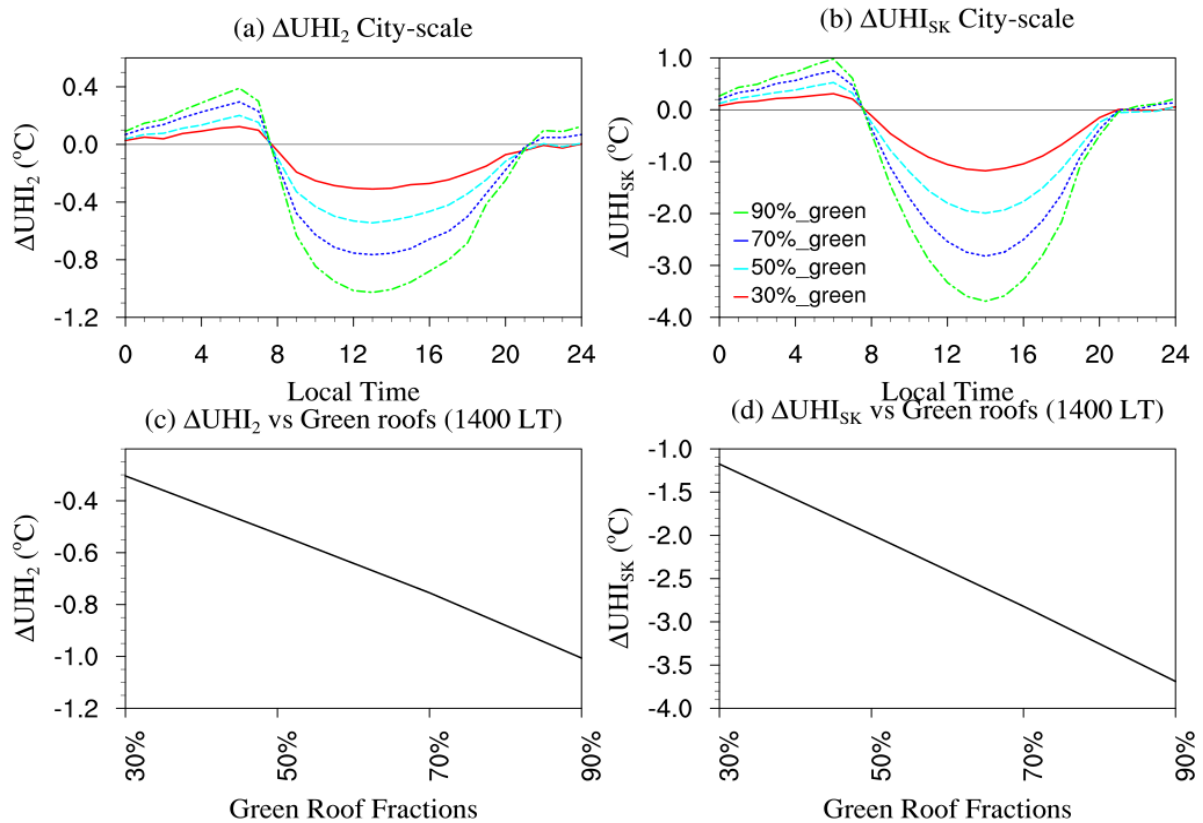


Figure 7. Diurnal variations of (a) near-surface UHI (ΔUHI_2) and (b) roof surface UHI (ΔUHI_{SK}) reductions by using green roof fractions of 30, 50, 70, 90%. (c) and (d) are the corresponding reductions of near-surface and roof surface UHI effects when the reductions reach their maxima. The UHI has been averaged over urban grid points only in domain d03 over the 3 days (from 28 – 30 January in 2009).

Figure 8 illustrates the effectiveness of different green roof fractions in mitigating the UHI effects for the three different urban categories (Figure 1(b)) between the central business district and surrounding urban suburbs. The roof surface and near-surface UHI reductions are shown for low-density urban, high-density urban and commercial/industrial areas. These three urban categories have different urban properties for vegetated and impervious surfaces in the UCM (Table 1). Over the low-density urban area, the maximum reductions of the near-surface UHI intensities are 0.30, 0.50, 0.70 and 0.90 $^{\circ}C$, and the roof surface UHI intensities are 1.0, 2.0, 2.7 and 3.5 $^{\circ}C$ during the day for green roof fractions of 30%, 50%, 70% and 90% respectively. High-density urban and commercial areas show reductions 0.40, 0.70, 1.0 and 1.4 $^{\circ}C$ for the near-surface UHI and 1.2, 2.5, 3.4 and 4.8 $^{\circ}C$ for the roof surface UHI by using the same percentages of green roof fractions. The high-density urban and commercial areas show higher reductions of the near-surface and roof surface UHI effects than the low-

density urban area during the day. This finding shows that the application of green roofs can considerably reduce the roof surface and near-surface UHI effects in denser impervious areas due to the larger size of roof areas. Importantly, both the roof surface and near-surface UHI in the early morning (0200 - 0700 local time) are elevated as compared to conventional roofs at both the city-scale (Figure 7) and the individual urban categories (Figure 8) while there are no substantial differences during the night (2100 - 0200 local time). The roof surface and near-surface UHI are elevated by 1°C and 0.40°C respectively in the early morning. According to Li *et al* (2014), near-surface moisture in the low-density urban area is substantially increased due to evapotranspiration from surrounding larger size pervious area. As a consequence, a vapor pressure deficit over the low-density urban area reduces evapotranspiration, which helps to increase the temperature in the vegetated surface (Li *et al* 2014). Overall, the warming effect at night is much lower as compared to the reductions in temperature during the day.

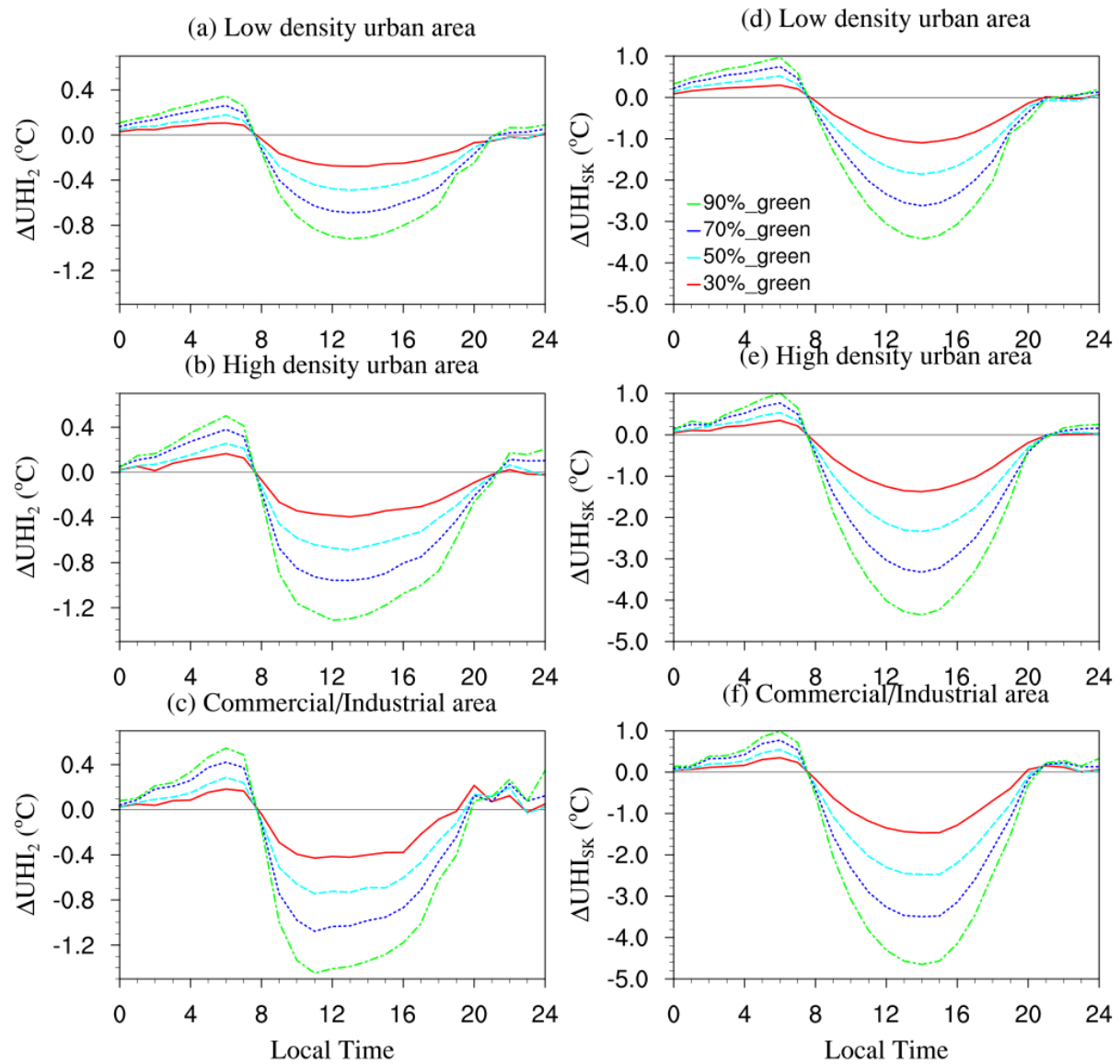


Figure 8. The near-surface (left panel) and roof surface (right panel) UHI reductions for low density, high density, and commercial/Industrial urban categories by using 30%, 50%, 70% and 90% green roof fractions.

Figure 9 shows the spatial differences in the roof surface UHI and wind speed at 10 m over the city of Melbourne by using 30%, 50%, 70% and 90% green roof fractions relative to conventional roofs, averaged from 1400 – 1800 local time over the 3 days simulation period. This time interval was chosen as it corresponds to the period when the roof surface temperature reaches its peak. Figure 9 (top panel) shows that the 30% and 50% green roof fractions can reduce the roof surface UHI from 1 to 2°C, while the 70% and 90% cool roof fractions can reduce the maximum UHI by 2 to 3°C and 3 to 4°C, respectively. The reductions in roof surface UHI increases with larger green roof fractions. Figure 9 (bottom panel) also shows that green roofs have a smaller effect on wind speed as the reductions of wind speed by the green roof fractions are lower. Green roofs reduce the maximum wind speed by up to 0.25 to 1.25 m s⁻¹ by increasing green roof fractions from 30% to 90%. Interestingly, wind speed increases by up to 0.75 m s⁻¹ over offshore areas. This is likely related to changes in roughness due to the vegetation on green roofs. It is also noteworthy that the impacts of green roofs are not substantial in non-urban areas.

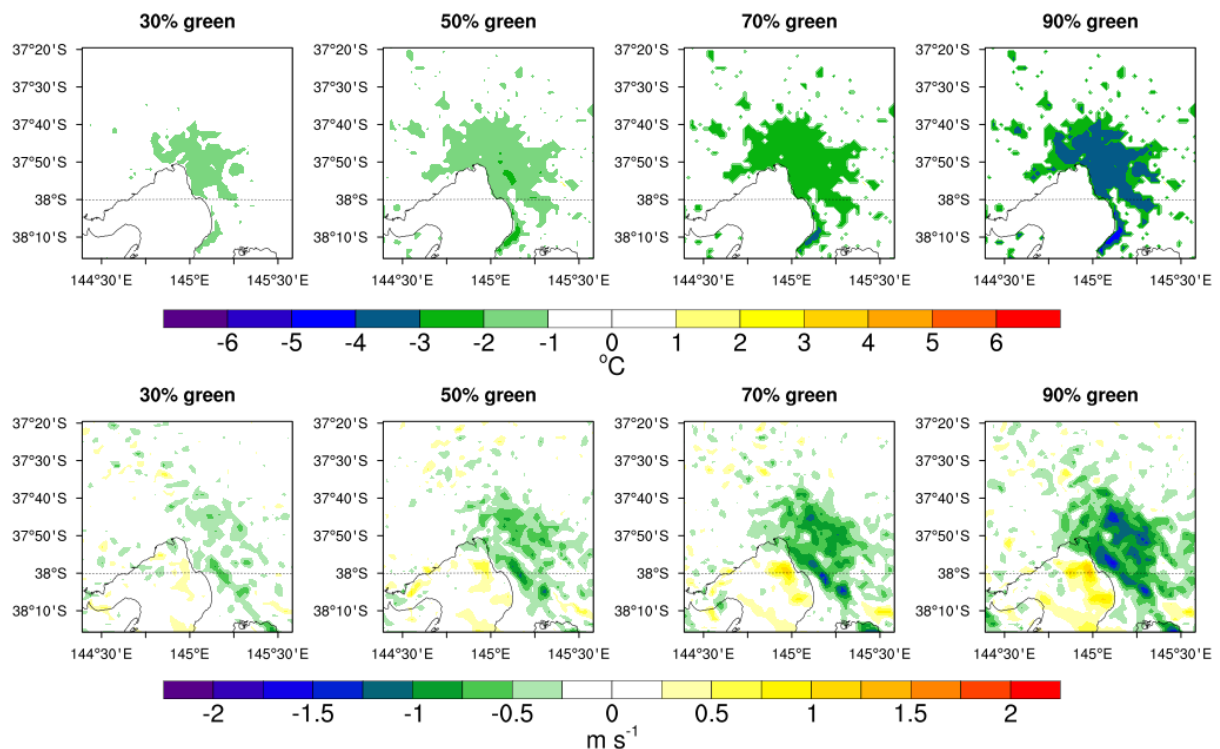


Figure 9. Changes of roof surface UHI (upper panel) and wind speed at 10 m (bottom panel) by using 30%, 50%, 70% and 90% green roof fractions. All the results are averaged from 1400 – 1800 local time for the 3 days (from 28 – 30 January in 2009) over domain d03 when roof surface temperature reaches its peak.

3.4. Effectiveness of cool roofs in mitigating UHI effects

The effectiveness of cool roofs in mitigating the UHI is assessed based on three numerical experiments by varying the albedo to 0.50, 0.70 and 0.85 for 100% cool roofs (the UCM model is designed for only 100% cool roofs). Figure 10 shows changes in the surface energy balance due to increased albedo. Cool roofs reduce daily average sensible heat flux by up to 100, 170 and 220 W m^{-2} by using the albedo values of 0.50, 0.70 and 0.85 respectively. Net radiation is also reduced by up to 100, 160 and 180 W m^{-2} (~ 4 times) as compared to the conventional roofs by using the same albedo values during the day due to substantial amount of incoming solar radiation being reflected back to the atmosphere. Cool roofs are more effective in reducing net radiation and consequently, sensible heat flux, as compared to green and conventional roofs, especially during the day. Although green roofs transform net radiation into latent heat flux due to evapotranspiration, the reduction in sensible heat flux is smaller as compared to the use of cool roofs. Interestingly, increasing albedo substantially reduces the latent heat flux in urban areas because of lower net radiation. In the UCM, 10% of urban grid cells are considered as a naturally vegetated surface. Therefore, the source of this latent heat flux must be from the naturally vegetated part of the urban grid cells. The reductions in storage heat of cool roofs are also similar to green roofs except in the morning (0700 – 1100 local time). However, the reductions of net reduction by cool roofs are considerably higher (120 W m^{-2}) than the green roofs during the day. The storage heat in the roofs re-radiates during the latter part of the day, or alternately, this heat can be transferred into the building indoor spaces and can increase the cooling energy demand for the air conditioners. Therefore, cool roofs and green roofs have the potential to reduce the cooling energy demand for buildings by reducing the storage heat, and consequently, reducing anthropogenic heat emissions in urban areas. Finally, cool roofs result in a substantial reduction in net radiation that is an important contributor in mitigating UHI effects. There are no substantial differences in the surface energy balance between cool and conventional roofs at night.

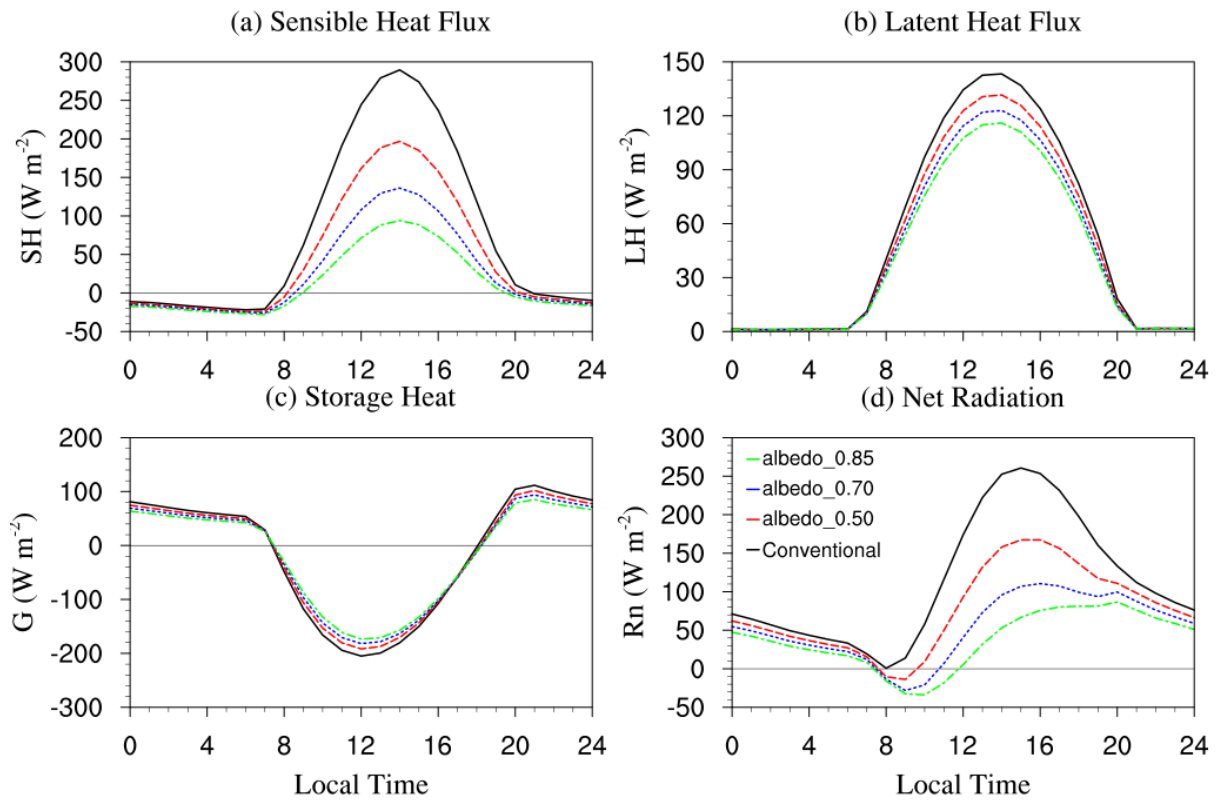


Figure 10. Diurnal variation of (a) sensible heat flux (b) latent heat flux, (c) storage heat, and (d) net radiation, averaged only over urban grid points in domain d03 over 3 days (from 28 – 30 January in 2009), for experiments with albedo values of 0.5, 0.7, and 0.85 for cool roofs and the control.

Figure 11 shows the near-surface and roof surface UHI reductions by using albedo values of 0.85, 0.70 and 0.50, and the relationship between the albedo values and UHI reductions. The higher albedo of cool roofs substantially reduces the roof surface and near-surface UHI effects during the day. City-scale maximum reductions of the near-surface UHI reach up to 0.60, 1.1 and 1.5°C, while roof surface UHI reductions are 2.2, 3.8 and 5.2°C by using albedos of 0.50, 0.70 and 0.85 respectively. Larger reductions of the roof surface UHI (1°C) and the near-surface UHI (0.50°C) are obtained by using cool roofs (albedo 0.85) as compared to 90% green roof fraction during the day (Figure 7). The effectiveness of cool roofs in reducing UHI effects is drastically reduced (2/3) when the albedo is lowered from 0.85 to 0.50. Interestingly, a slight non-linear relationship is obtained between the UHI reductions and increasing albedo values of cool roofs (Figures 11(c) and 11(d)) as compared to green roofs (Figures 7(c) and 7(d)).

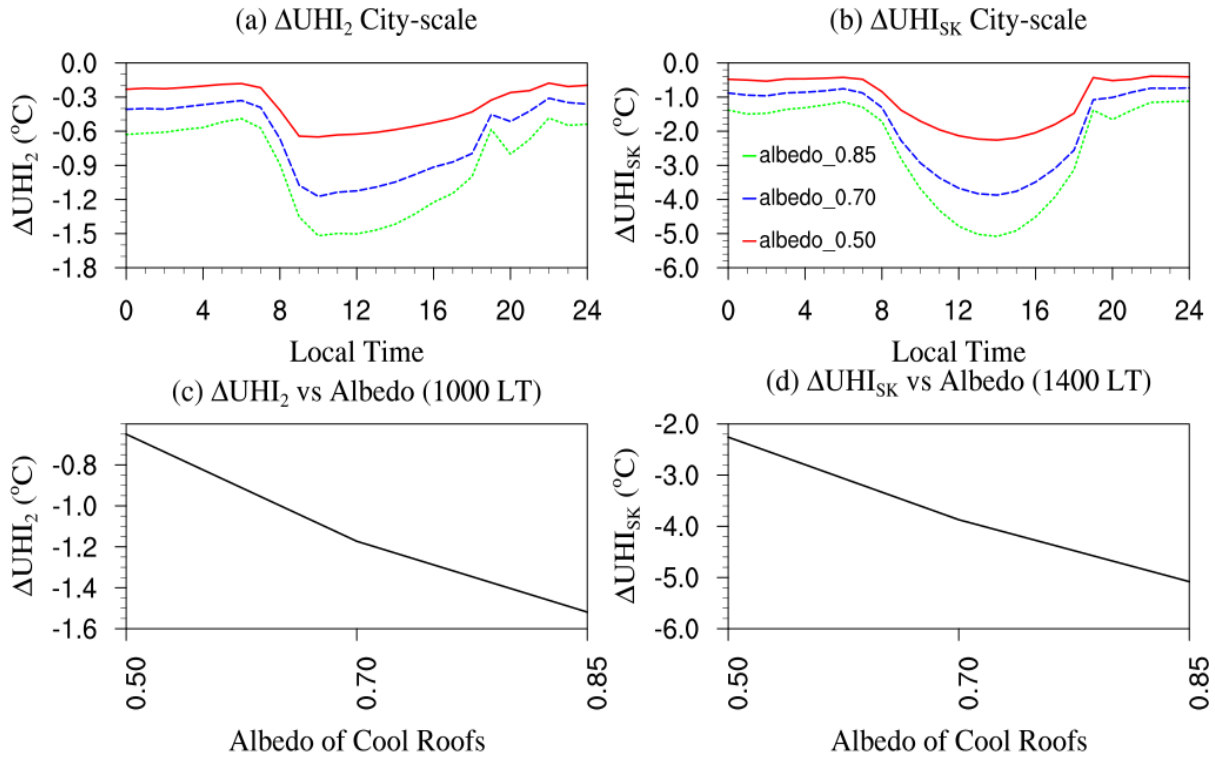


Figure 11. Diurnal variations of (a) near-surface UHI (ΔUHI_2) and (b) roof surface UHI (ΔUHI_{sk}) reductions by using albedo values of 0.5, 0.7, and 0.85 for cool roofs. (c) and (d) are the corresponding reductions of near-surface and roof surface UHI effects when the reductions reach their maxima. The UHI has been averaged over urban grid points only in domain d03 over the 3 days (from 28 – 30 January in 2009).

Figure 12 shows the effectiveness of cool roofs in reducing both the roof surface and near-surface UHI effects for the different urban categories in the city center and surrounding low-density urban areas (Figure 1 (b)). The reductions in the near-surface UHI are 0.50, 1.0 and 1.4 $^{\circ}C$ in the low-density urban areas during the day while the roof surface UHI reductions are 2.2, 3.6 and 5.0 $^{\circ}C$ by using albedos of 0.50, 0.70 and 0.85 respectively. During the day, cool roofs can reduce the near-surface UHI by 0.80, 1.5 and 2.2 $^{\circ}C$ and the roof surface UHI by 2.4, 4.2 and 5.8 $^{\circ}C$ in the high-density urban and commercial areas by using the same albedo. The cooling effect of cool roofs is larger in the high-density urban and commercial/industrial areas than the low-density urban area because of the larger roof areas (90 – 95%) in the high-density and commercial/commercial areas. When the albedo is reduced from 0.70 to 0.50 and 0.85 to 0.70, the cooling effects of cool roofs are reduced by up to 0.70 $^{\circ}C$ for near-surface temperature in both high-density urban and commercial areas, and 1.8 $^{\circ}C$ and 1.6 $^{\circ}C$ for the roof surface UHI in high-density urban and commercial areas, respectively. These results suggest that cool roofs may need a higher degree of maintenance for maintaining a high albedo by preventing dirt accumulation on the roof surfaces.

When considering all urban categories (Figure 11) and each urban category separately (Figure 12), a cool roof strategy results in larger reductions of the roof surface and near-surface UHI effects in the early morning and the night as compared to using green roofs

(Figures 7 and 8). This finding suggests that cool roofs extend the daytime cooling effect into the night by reducing heat storage in the roofs during the day, which is consistent with the study of Li *et al* (2014). A similar result has been reported by Georgescu *et al* (2014), who have shown that cool roofs are more effective than green roofs in reducing the UHI.

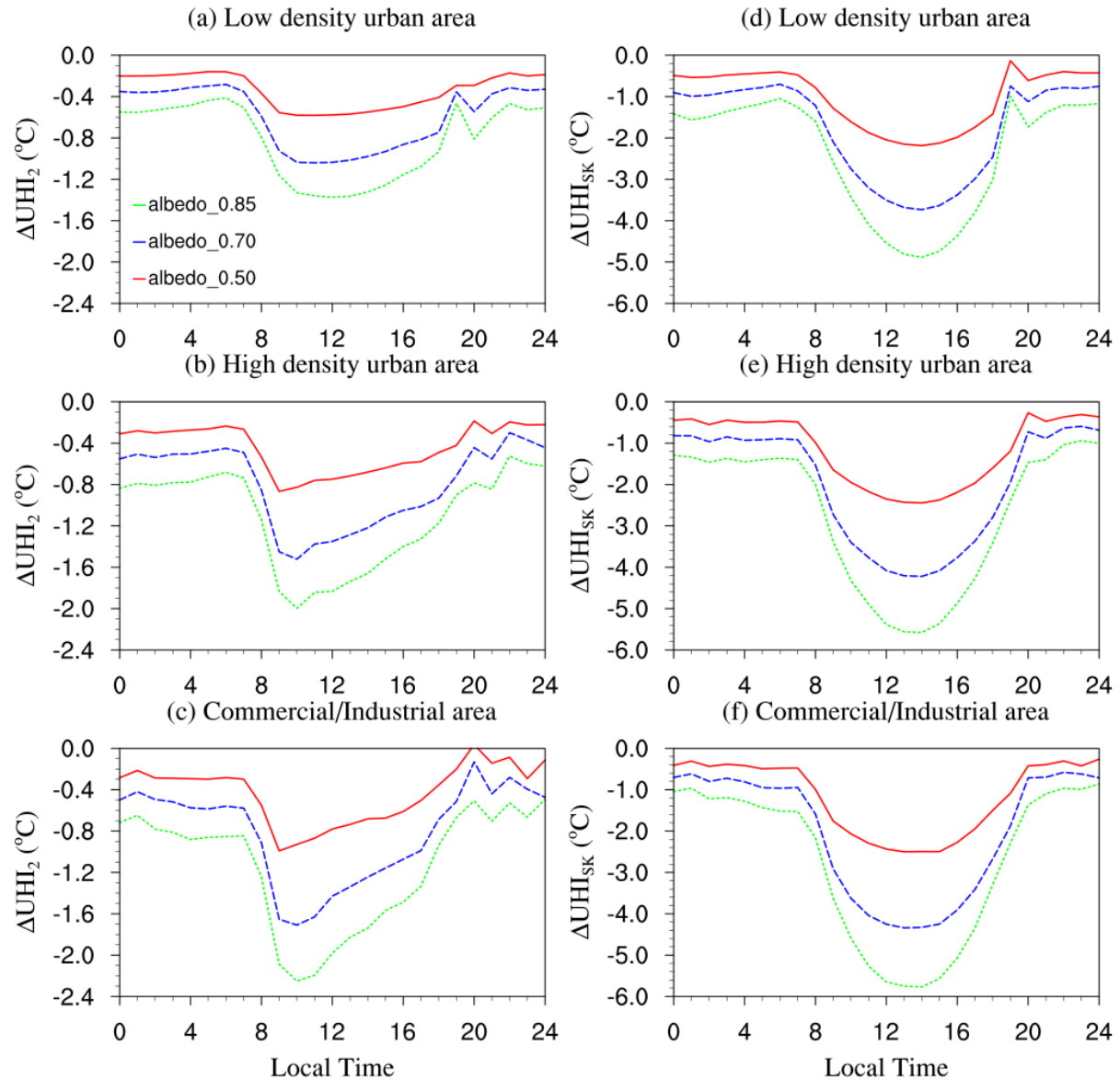


Figure 12. Diurnal variation of the near-surface (left panel) and roof surface (right panel) UHI reductions for low density (a and b), high density (b and c) and commercial areas (c and f) by using albedo values of 0.50, 0.70 and 0.85 for cool roofs.

In summary, it is notable that the substantial direct thermal impacts of green and cool roofs on roof surface temperature for both the city-scale and different urban categories happens during the afternoon (1200 – 1600 local time), which is nearly the same time when the daily roof surface temperature reaches its peak at 1500 local time (Figure 5). On the other hand, the maximum direct thermal impacts of green and cool roofs for near-surface temperature occurs earlier between 900 and 1300 local time, but the near-surface temperature reaches its daily peak later at 1700 local time. Hence, the effectiveness of green and cool roofs in reducing

the near surface temperature is limited as near surface temperatures are largely driven by properties of the land surface.

Figure 13 shows the changes in roof surface UHI (upper panel) and the wind speed at 10 m (bottom panel) for different albedos with 100% cool roofs as compared to conventional roofs. Cool roofs can reduce the maximum roof surface UHI by up to 3, 4 and 5°C in urban areas for albedos of 0.50, 0.70 and 0.85 respectively. The reductions of the roof surface UHI depends on the magnitude of the albedo, with higher albedo leading of higher amount of reflection of incoming shortwave radiation, and consequently, higher reductions of UHI effects. The reductions in wind speed by using cool roofs are also lower (0.5 – 1.75 m s⁻¹) in urban areas, but higher than the green roofs. On the other hand, cool roofs increase the wind speed (0.50 – 1.0 m s⁻¹) over offshore areas. As would be expected, the impacts of cool roofs in reducing the roof surface UHI and changing the wind speed are always higher in the center of the city.

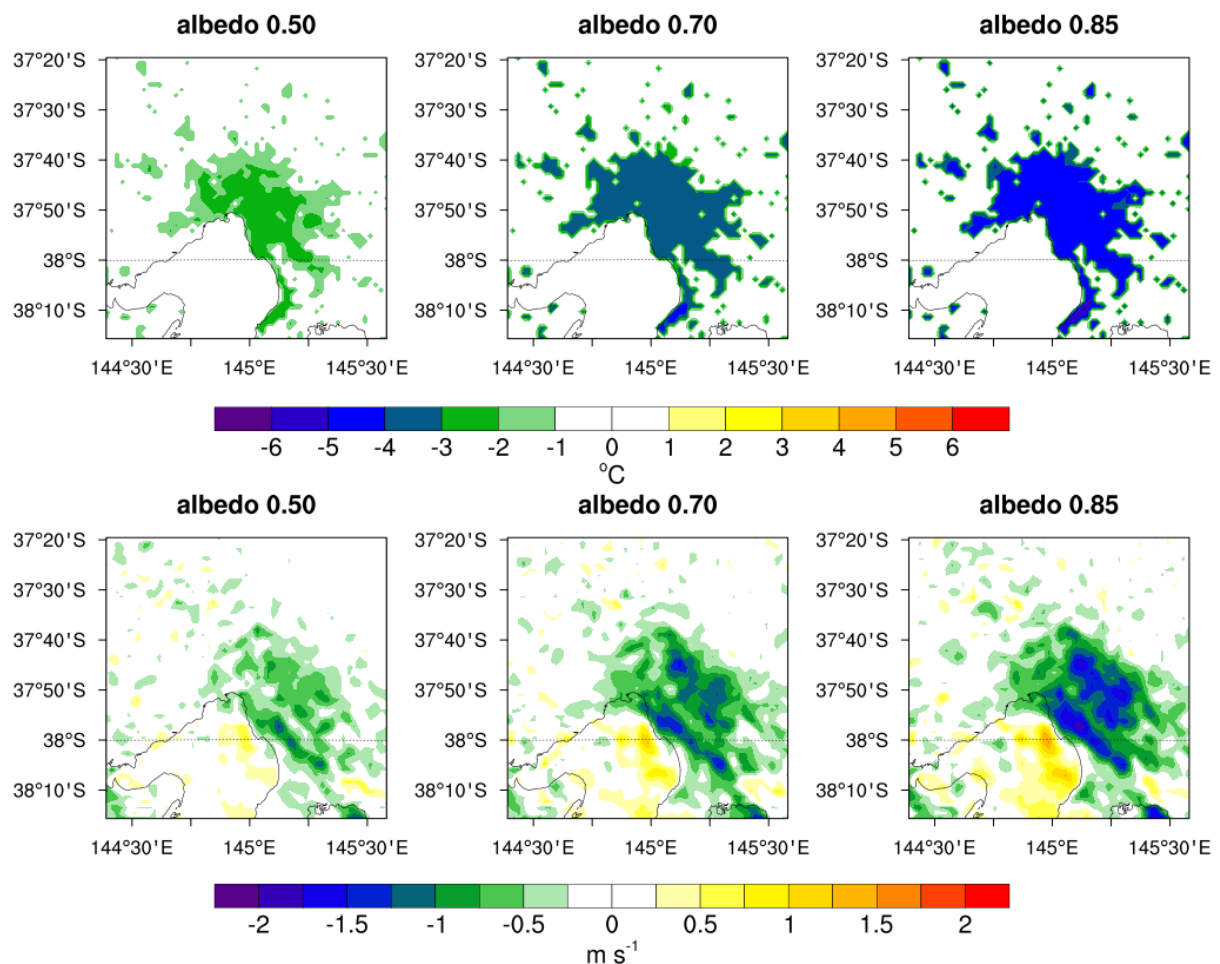


Figure 13. Changes of roof surface UHI (upper panel) and wind speed at 10 m (bottom panel) by using albedo values 0.50, 0.70 and 0.85 for cool roofs. All the results are averaged from 1400 – 1800 local time for the 3 days (from 28 – 30 January in 2009) over domain d03 when roof surface temperature reaches its peak.

3.5 Influence of initial soil moisture

All the simulations discussed so far use the WRF default initial soil moisture of $0.20 \text{ m}^3 \text{ m}^{-3}$ for the green roofs. To investigate the effects of initial soil moisture, two additional simulations were carried out by setting up initial soil moisture to 0.30 and $0.40 \text{ m}^3 \text{ m}^{-3}$ for the experiment with 50% green roof fraction. An additional simulation was carried out using a lower initial soil moisture $0.15 \text{ m}^3 \text{ m}^{-3}$ in order to examine the performance of 50% green roofs under dryer conditions. The impacts of initial soil moisture on green roofs are examined based on the ability of green roofs in reducing near-surface and roof surface UHI effects where the 50% green roof experiment is the control simulation. Figure 14 shows that changing initial soil moisture conditions did not have a sustained effect on the UHI. Although the increased initial soil moisture in green roofs slightly reduces the near-surface UHI (maximum 0.015°C) and the roof surface UHI (maximum 0.03°C) during the day, the maximum near surface and roof surface UHI during the morning and night are elevated by up to 0.03°C and 0.15°C respectively as compared to the 50% green roofs. On the other hand, using drier initial soil conditions ($0.15 \text{ m}^3 \text{ m}^{-3}$) for green roofs increases warming effect during both the day and night. The near-surface UHI increases by up to 0.042°C during the night while the roof surface UHI is elevated by up to 0.06°C as compared to the 50% green roofs. Hence, the effect of initial soil moisture in green roofs is not substantial in reducing near-surface and roof surface UHI effects for this case study. This is likely due to the very hot and dry conditions quickly evaporating any excess soil moisture, consistent with the study by Kala et al. (2015) who investigated the effects of higher initial soil moisture during the same heat-wave event.

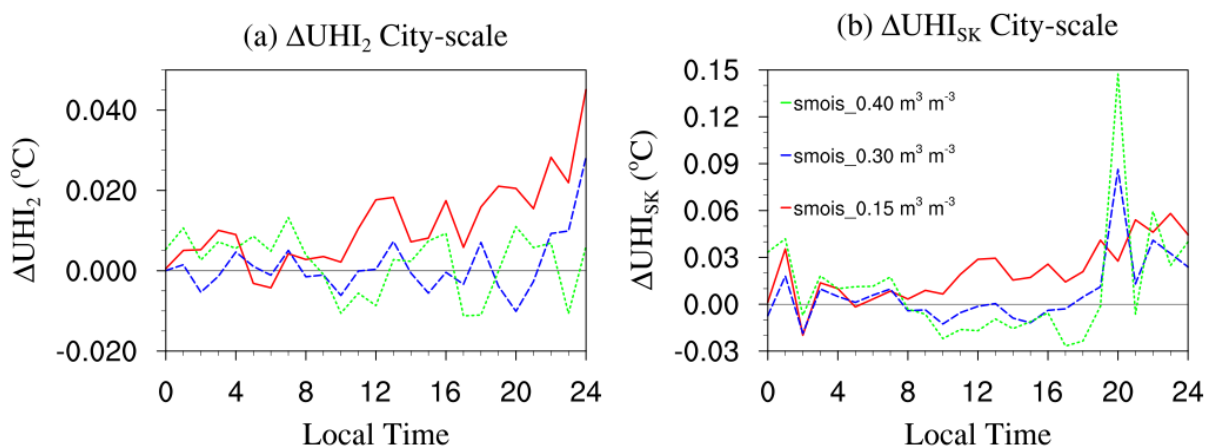


Figure 14. Diurnal variations of (a) near-surface UHI (ΔUHI_2) and (b) roof surface UHI ($\Delta\text{UHI}_{\text{SK}}$) as a function of green roof soil moisture (experiments with 50% green roof fraction). The UHI has been averaged over urban grid points only in domain d03 over the 3 days (from 28 – 30 January in 2009).

3.6. Effects of green and cool roofs on boundary layer

Figure 15 shows the changes in air temperature, winds (rotated to earth coordinates) and relative humidity in the boundary layer averaged over urban areas for 90% green roofs and cool roofs (albedo 0.85) as compared to conventional roofs over 3 days from 28 – 30 January in 2009. The maximum air temperature is reduced by up to 0.4°C and 0.6°C by using green and cool roofs respectively in the lower boundary layer during the day. Interestingly, the reduction in air temperature for cool roofs extends up to 1.8 km within the PBL, while the reduction for green roofs is only up to 0.9 km. The magnitude of the reduction in air temperature by cool roofs are higher by up to 0.2°C as compared to green roofs. The maximum reduction in wind speed (1 m s^{-1}) occurs in the lower boundary layer for green and cool roofs during the late afternoon on the 28th and 30th January. However, the changes in wind speed are not substantial for the remaining hours in both lower and upper boundary layer as compared to conventional roofs. Furthermore, both green and cool roofs demonstrate no substantial changes in relative humidity as compared to conventional roofs in the lower boundary layer. This finding suggests that the changes in relative humidity as a result of evapotranspiration are not substantial because of the dry and hot conditions during the heatwave event. This finding is not consistent with previous studies. For example, Li *et al* (2014) report higher relative humidity in urban areas because of stronger advection of moist air from rural areas. Similarly, Sharma *et al* (2016) report higher relative humidity for green roofs because of higher evapotranspiration and lower winds, and higher relative humidity for cool roofs due to the reduced temperature and moist cool air from surrounding rural areas. However, based on the analyses of vertical profiles of temperatures, winds and relative humidity of green and cool roofs, this study suggests that the advection of moist air from rural areas is unlikely to be the driving mechanism due to the extremely hot and dry conditions during the heatwave event. Another mechanism could be convective rolls due to heated urban surfaces and higher roughness of the urban areas.

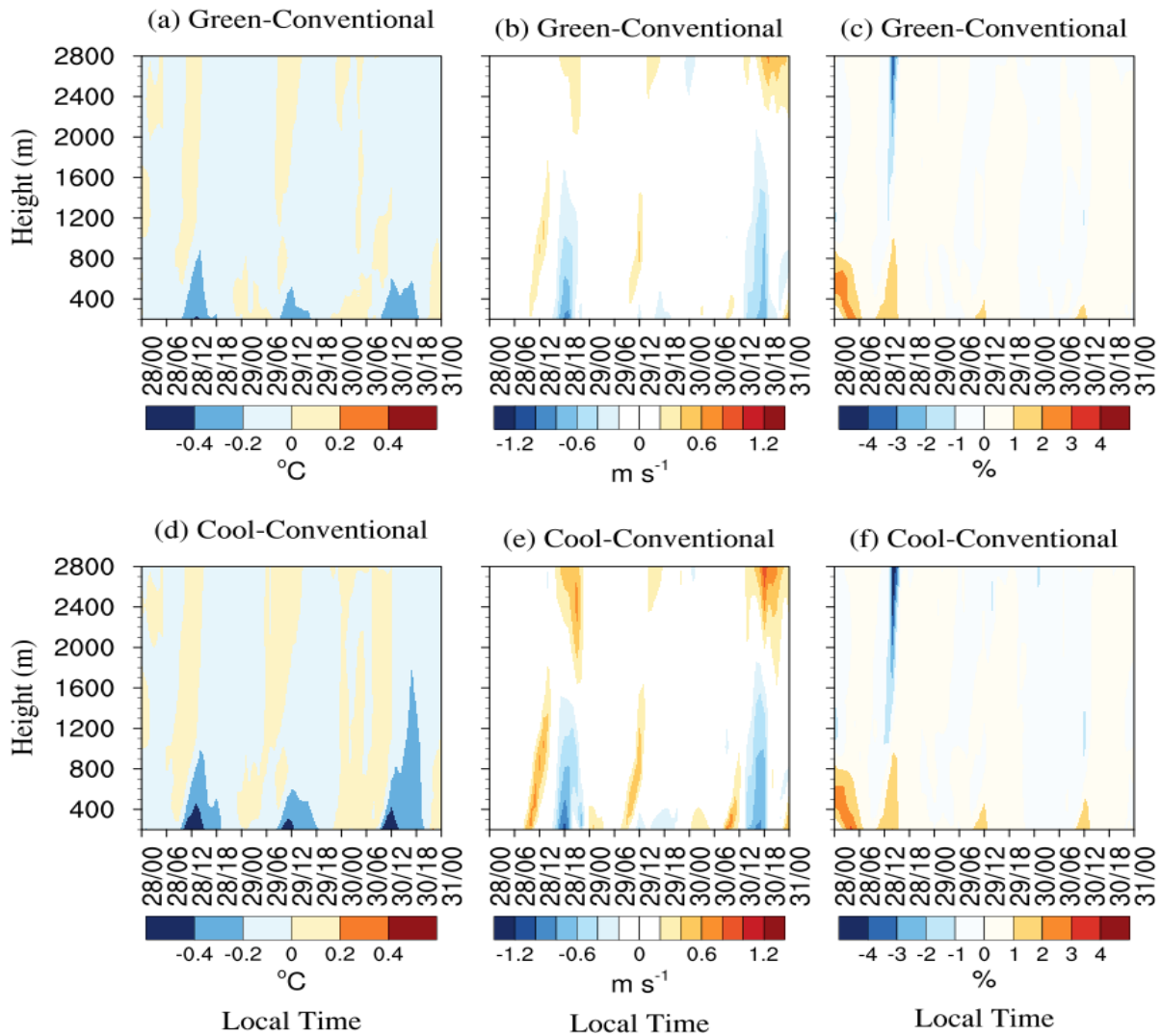


Figure 15. The differences between green and conventional roofs (top) and cool and conventional roofs (bottom); (a) and (d) are the changes of air temperature; (b) and (e) are the changes of wind speed; (c) and (f) are the changes of relative humidity averaged over urban grid cells for green and cool roofs for the 3 days from 28 – 30 January.

To investigate the influence of convective rolls, it is useful to examine changes in the vertical wind component as well as turbulence. Vertical wind speeds are shown in Figures 16(a) to 16(c) while Turbulent Kinetic Energy (TKE) are shown in Figures 16(d) to 16(f) for conventional, 90% green roofs and cool roofs (albedo 0.85) over 3 days from 28 – 30 January in 2009. Finally, the planetary boundary layer heights (PBLH) are illustrated in Figure 16(g) for the same experiments. The vertical wind speed, TKE and PBLH are important factors for indicating the strength of vertical mixing. Figure 16(a) illustrates that the conventional roofs show stronger vertical wind speed on the 28th and 30th January, which indicates vertical transport of energy fluxes (e.g., latent and sensible heat fluxes) from surface to higher boundary layer. Furthermore, green and cool roofs (Figures 16(b) and 16(c)) also indicate positive vertical wind speed with smaller reductions as compared to conventional roofs in most cases except on the 29th January which also indicates vertical transport of energy. Figures 16(d) and 16(f) show that green and cool roofs result in a decrease in TKE from 0.2

to $1.5 \text{ m}^2 \text{ s}^{-2}$ during the day, while conventional roofs show the highest TKE ranging from 0.2 to $1.9 \text{ m}^2 \text{ s}^{-2}$. Both the vertical wind speed and the TKE results indicate that the conventional roofs result in stronger vertical mixing during the day as compared to green and cool roofs, which show reductions in the vertical wind speed and TKE. The prevalence of vertical mixing in all experiments is due to the strong surface heating during the heatwave event. These findings are consistent with the reduction in sensible heat fluxes by green and cool roofs (Figures 6(a) and 10(a)). Green roofs reduce PBLH by up to 180 m as compared to conventional roofs while cool roofs reduce the maximum PBLH by 300 m over urban areas (Figure 16(g)). In general, lower sensible heat flux reduces vertical mixing and reduces vertical wind speed, and consequently, the PBLH is shallower. Figures 16(b) and 16(c) illustrate that green and cool roofs slightly reduce vertical wind speeds, and consequently, generate lower PBLH due to lower sensible heat flux. Similar results have been obtained by Georgescu (2015) and Sharma *et al* (2016), who have shown that lower sensible heat flux generated by green and cool roofs leads a reduction in vertical mixing and the lower PBLH.

Li *et al* (2014) reported that the advection of moist air from rural to urban areas occurs due to weaker vertical mixing over urban areas, and consequently, the atmosphere beyond a given height over urban areas is not affected by surface conditions. The much weaker vertical mixing further enables the development of stronger advection. However, this study did not obtain stronger advection of moist air from rural areas (Figures 15(c) and 15(f)) and this is most likely because of the considerable vertical mixing for green and cool roofs over urban areas (Figure 16(b) and 16(c)). In general, vertical mixing helps to develop horizontal convective rolls over urban areas. As a result, the urban atmosphere is strongly affected by the surface conditions in urban areas during heatwave events. Figures 16(a) to 16(f) suggest that the heated surfaces in the urban areas are the main influencing factor for controlling vertical wind speed and TKE that enhances in developing larger convective rolls over urban areas. According to (Miao *et al* 2009), the development of convective rolls is enhanced when the vertical wind speed is stronger. Based on the vertical wind speed and TKE analyses for green and cool roofs, the result indicates the stronger influence of convective rolls on the urban atmosphere during heatwave conditions. This is another important finding of this study as compared to previous studies, which reported that the synoptic or mesoscale wind plays an important role for the advection of moist air from rural areas into urban areas (Li *et al* 2014, Sharma *et al* 2016).

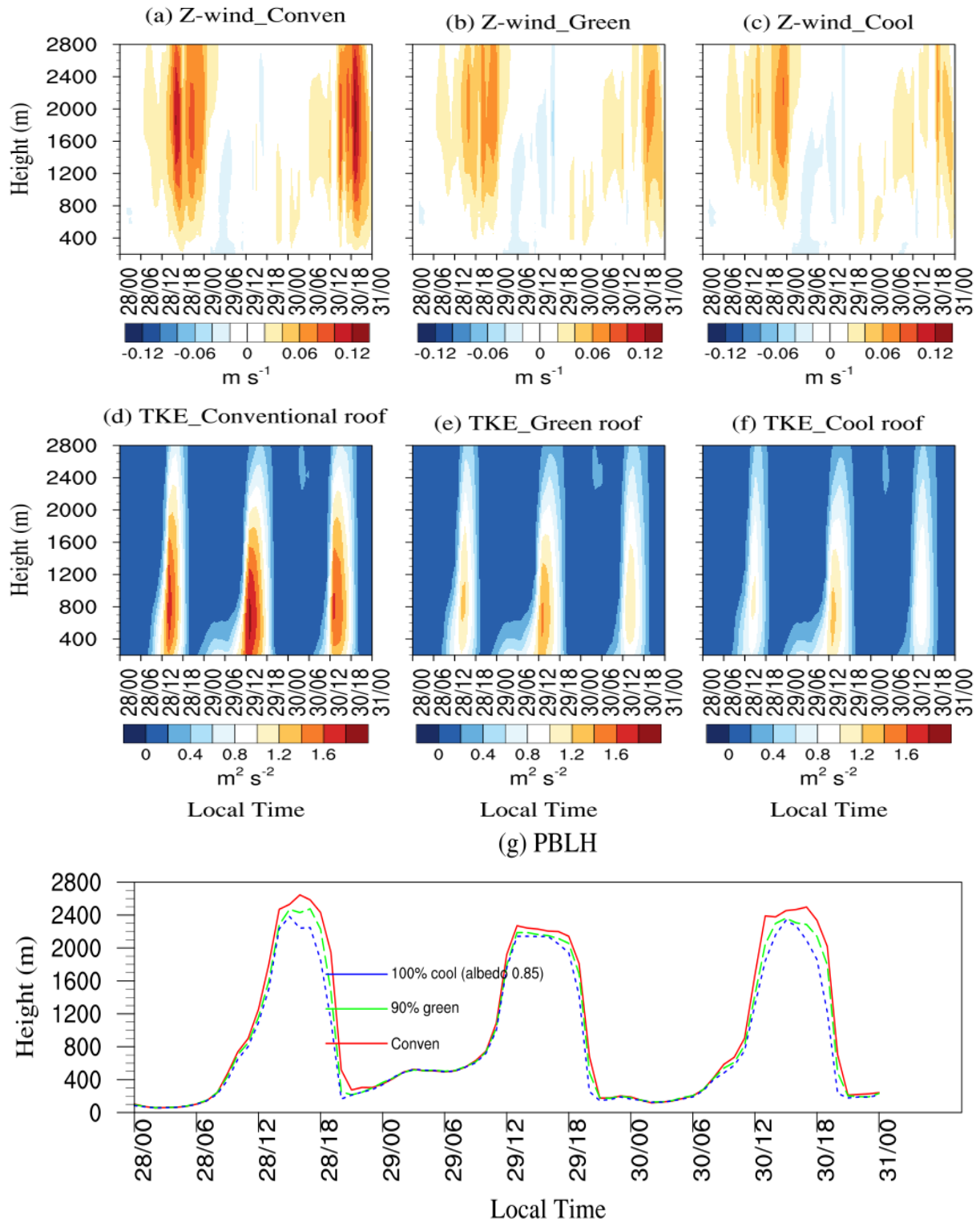


Figure 16. Vertical wind speed for (a) conventional roofs, (b) 90% green roofs and (c) cool roofs with albedo of 0.85. TKE for (d) conventional roofs, (e) green roofs (f) cool roofs. Temporal variations of PBLH for (g) conventional, green and cool roofs.

3.7. Effects of green and cool roofs on human thermal comfort

Figure 17 shows the control (top panel) and changes in human thermal stress via UTCI index at pedestrian and roof-surface levels (middle and bottom panels). The improvement in HTC are smaller at pedestrian level/near-surface (2 m) for both green and cool roofs. However, the HTC is noticeably improved by reducing of the UTCI index at roof-surface level during the day. For pedestrian level UTCI, using 50% and 90% green roofs result in reductions of the maximum UTCI by up to 0.60°C and 1.5°C during the day, respectively, while cool roofs with albedos of 0.50 and 0.85 lead to reductions in the maximum UTCI by 1°C and 2.4°C respectively. At roof-surface level, the maximum reductions of the UTCI are 2.8°C and 5.7°C by using 50% and 90% green roofs, and 3.2°C and 8°C by using an albedo of 0.50 and 0.85 for cool roofs, respectively. Green and cool roofs are very effective in reducing the UTCI index from extreme (UTCI>46 °C) to very strong (UTCI>38 °C) at roof-surface level during the day according to the classification presented in Table 3. Interestingly, cool roofs always result in a higher UTCI reduction than the green roofs, while 90% green roofs and cool roofs with an albedo of 0.85 show almost similar reductions of the UTCI. It is noteworthy that at night, cool roofs also reduce the UTCI while green roofs increase the UTCI, but the changes are small. Cool roofs are more efficient than green roofs in improving HTC during the day because of higher reflection of incoming solar radiation. Green and cool roofs substantially improve the HTC at rooftop-podium level as compared to the pedestrian level as the temperature reductions are much higher at the roof-surface level than the near surface. This finding suggests that green and cool roofs result in smaller changes to the pedestrian level HTC due to the additional reflective radiation from building facades and impervious surfaces at the surface. This is expected as green and cool roofs are unlikely to affect the energy balance at pedestrian level due the considerable distance between roof-surface and near-surface levels, and consequently, this result in only minor improvements for the pedestrian level HTC. It is also noteworthy that green and cool roofs are able to reduce heat stress, even when very strong and extreme heat stress occurs at pedestrian and roof surface level respectively during the day. Furthermore, the differences in wind speed and relative humidity between conventional and green and cool roofs are small (Figure 15), but the differences in sensible heat and latent heat fluxes are substantial (Figures. 6 and 10) for green roofs while the differences in sensible flux are higher for cool roofs. Therefore, the sensible and latent heat fluxes play a key role in controlling HTC for green roofs while sensible heat flux is the key driving factor in improving HTC for cool roofs during heatwave.

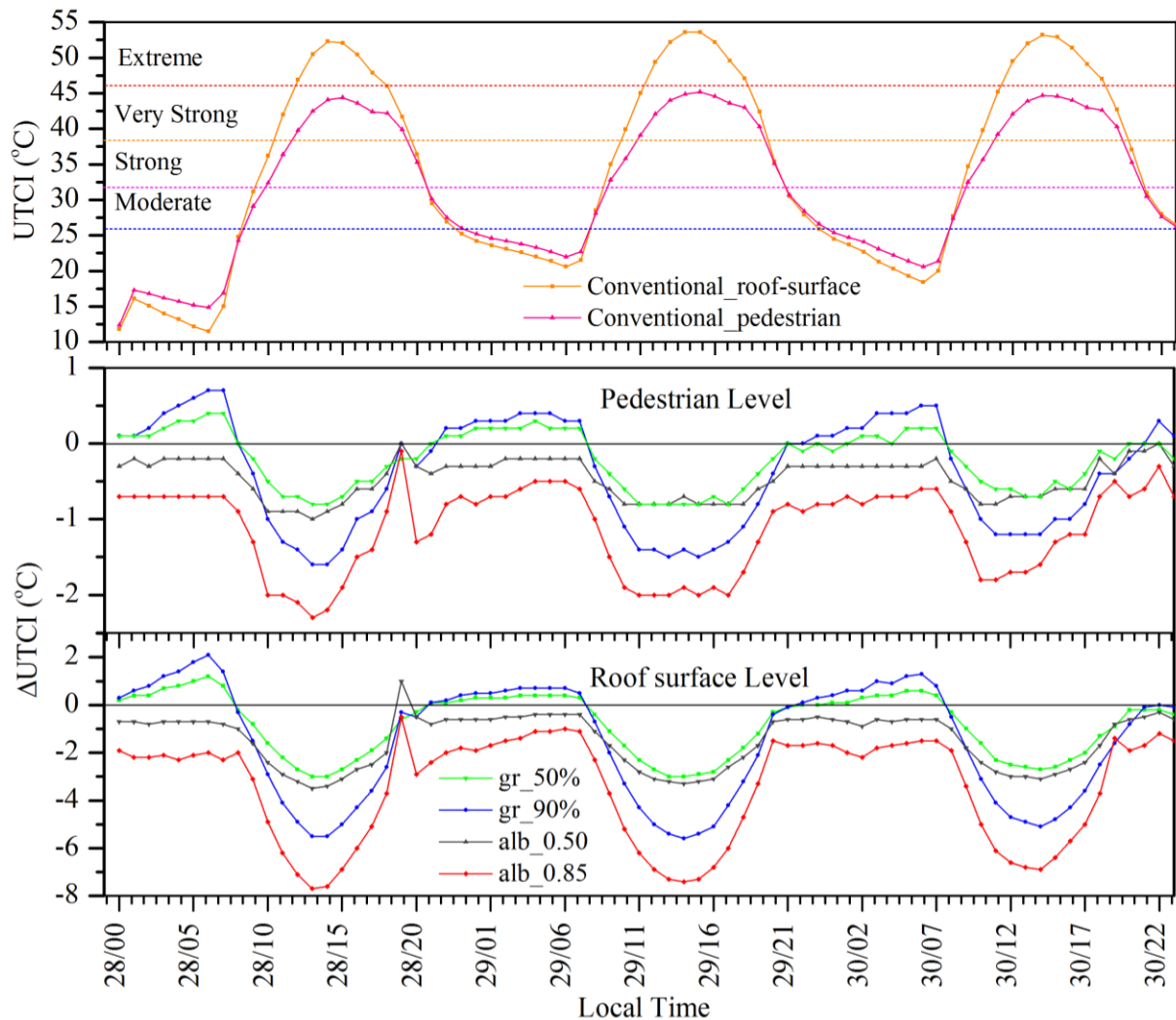


Figure 17. Hourly time series of HTC in pedestrian and roof-surface levels for conventional roofs (top). The changes of HTC in near-surface (middle) and roof surface (bottom) levels for green and cool roofs. HTC effects represented by the UTCI index. All results are averaged over only urban grid points in domain d03 for the 3 days (from 28 – 30 January in 2009).

4. Conclusions

Heatwave events exacerbate UHI effects, and the frequency and intensity of heatwaves are increasing in southeast Australia. Therefore, it is critical to investigate the effectiveness of mitigation strategies such as the use of green and cool roofs. To address this important question, this study evaluates the effectiveness of green and cool roofs in mitigating UHI effects and improving HTC in the city of Melbourne during an extreme heatwave event from the 27th to 30th of January 2009 using the WRF-UCM model.

The UHI reductions vary linearly with the increasing green roof fractions, but slightly non-linear with the increasing albedo of cool roofs. The roof surface UHI is reduced from 1.15°C to 3.8°C when green roof fractions are increased from 30% to 90%. Furthermore, cool roofs result in maximum reductions of the roof surface UHI ranging from 2.2 to 5.2°C by

increasing the albedo from 0.50 to 0.85, which is a larger reduction by approximately 1.4°C as compared to 90% green roofs. The impacts of green and cool roofs varied for the different urban categories with reductions of the roof surface UHI by green roofs ranging from 1 to 3.5°C in low-density urban areas, and 1.2 to 4.6°C in the high-density urban and the commercial/industrial areas. Similarly, the reductions due to cool roofs ranged from 2.2 to 5.0°C in the low-density urban areas, and 2.4 to 5.8°C in the high-density urban and the commercial/industrial areas. The high density and commercial/industrial areas experienced larger UHI reductions because of larger areas of cool roofs. Furthermore, increasing soil moisture did not have a substantial influence in reducing UHI effects. However, soil moisture deficit on green roofs can exacerbate the UHI effects during both the day and night.

The green roofs and cool roofs not only alter the surface energy balance and reduce the UHI effects but also influence the boundary layer up to 2.5 km. The decrease in sensible flux due to the green and cool roofs reduces vertical mixing and the PBLH, and consequently, reduces the air temperature. However, the changes in wind speed and relative humidity are not substantial in the lower boundary layer during the day. Green and cool roofs decrease the sensible heat flux and consequently reduce vertical mixing, the depth of boundary layer and temperatures over urban areas in the lower atmosphere, which reduces UHI effects. Cool roofs reflect the incoming solar radiation, and consequently, decrease the sensible heat flux and reduce UHI effects. Green roofs provide heat transfer benefits via evapotranspiration. Nonetheless, green roof approach has a limitation particularly in the early morning because of increased UHI effects. This problem might be overcome by applying an optimal strategy including the appropriate mix of vegetation on green roofs and cool roofs, and this requires further study.

Green and cool roofs substantially improve HTC at the roof surface level but this effect is much smaller at the pedestrian level. Both green and cool roofs are effective in improving HTC by reducing the UTCI index from extreme ($UTCI > 46^\circ\text{C}$) to very strong ($UTCI > 38^\circ\text{C}$) at roof surface level although the improvement of HTC at pedestrian level is not substantial. Interestingly, green and cool roofs show their potential in reducing thermal stress during the day when the worst (very strong to extreme) thermal stress occurs. This finding reflects the potential of green and cool roofs in reducing heat related illness and offering comfortable recreational and amenity spaces for the urban dwellers.

Our results also indicate that the physical processes/mechanisms involved in altering boundary layer structure and reducing UHI effects interact differently based on the characteristics of heatwave conditions as compared to regular summer days and geographical locations for green and cool roofs. Based on the analyses of vertical profiles of air temperature, wind and relative humidity, this study suggests that the advection of moist air from rural areas is unlikely to be the driving mechanism in boundary layer dynamics due to the extremely hot and dry conditions during the heatwave event. Furthermore, the study investigates the influence of convective rolls by examining the changes in the vertical wind component and TKE, which indicates the stronger influence of convective rolls on the urban boundary layer dynamics during heatwave conditions because of heated urban surfaces.

Finally, the study has some important inherent limitations which are important to discuss. While our study shows that cool and green roofs have potential to reduce UHI effects, implementing 90% green roofs, and having 100% of roofs with high albedos of up to 0.85 is not likely to be practically feasible across an entire city. The aim of this study was to investigate the maximum response, and this provides useful information, however, this does not necessarily translate to practical implementation. Additionally, the WRF-SLUCM model has inherent limitations in how buildings are represented in the model, for example, extensive (depth < 150 mm) versus intensive (depth > 150 mm) roofs and pitched versus flat roofs may have different effects on the surface energy balance, and this cannot be resolved by the model. Nonetheless, this study provides useful findings on the maximum expected response due to cool and green roofs at the large scale, and these findings are relevant for other cities which experience similar weather conditions during summer.

Acknowledgements

Data support by the Bureau of Meteorology (BoM) Australia and ECMWF (ERA-interim) data server (<http://apps.ecmwf.int/datasets/data/interim-full-daily/levtype=ml/>) are gratefully acknowledged. Authors also acknowledge Stephanie Jacobs and Carlo Jamandre for providing urban categories data (Jackson et al. (2010)) for the city of Melbourne. Jatin Kala is supported by an Australian Research Council Discovery Early Career Researcher Award (DE170100102). The comments from two anonymous reviewers helped to improve this manuscript. All of this assistance is gratefully acknowledged.

References

- Akbari H, Matthews H D and Donny S (2012) The long-term effect of increasing the albedo of urban areas *Environmental Research Letters*. 7 2 024004
- Akbari H, Shea Rose L and Taha H (2003) Analyzing the land cover of an urban environment using high-resolution orthophotos *Landscape and Urban Planning*. 63 1 1-14
- Argueso D, Evans J P and Fita L (2014) Temperature response to future urbanization and climate change *Climate Dynamics*. 42 7 2183-2199. doi.org/10.1007/s00382-013-1789-6
- Blazejczyk K, Epstein Y, Jendritzky G, Staiger H and Tinz B (2012) Comparison of UTCI to selected thermal indices *International Journal of Biometeorology*. 56 3 515-535
- Bröde P, Fiala D, Błażejczyk K, Holmér I, Jendritzky G, Kampmann B, Tinz B and Havenith G (2012a) Deriving the operational procedure for the Universal Thermal Climate Index (UTCI) *International Journal of Biometeorology*. 56 3 481-494
- Bröde P, Krüger E L, Rossi F A and Fiala D (2012b) Predicting urban outdoor thermal comfort by the Universal Thermal Climate Index UTCI—a case study in Southern Brazil *International Journal of Biometeorology*. 56 3 471-480
- Carson T B, Marasco D E, Culligan P J and McGillis W R (2013) Hydrological performance of extensive green roofs in New York City: observations and multi-year modeling of three full-scale systems *Environmental Research Letters*. 8 2 024036

- Chen F and Dudhia J (2001) Coupling an Advanced Land Surface–Hydrology Model with the Penn State–NCAR MM5 Modeling System. Part II: Preliminary Model Validation *Monthly Weather Review*. 129 4 587-604
- Chen F, Kusaka H, Bornstein R, Ching J, Grimmond C S B, Grossman-Clarke S, Loridan T, Manning K W, Martilli A, Miao S, Sailor D, Salamanca F P, Taha H, Tewari M, Wang X, Wyszogrodzki A A and Zhang C (2011) The integrated WRF/urban modelling system: development, evaluation, and applications to urban environmental problems *International Journal of Climatology*. 31 2 273-288
- Climate Institute (2013) Infrastructure Interdependencies and Business-Level Impacts Report. The Climate Institute, 2013.
<http://www.climateinstitute.org.au/articles/publications/infrastructure-interdependenciesand-business-level-impacts.html>
- Coutts A, Beringer J and Tapper N (2007) Impact of Increasing Urban Density on Local Climate: Spatial and Temporal Variations in the Surface Energy Balance in Melbourne, Australia *J. Appl. Meteor. Climatol.* 46 477–493. <https://doi.org/10.1175/JAM2462.1>
- Cowan T, Purich A, Perkins S, Pezza A, Boschat G and Sadler K (2014) More Frequent, Longer, and Hotter Heat Waves for Australia in the Twenty-First Century *Journal of Climate*. 27 15 5851-5871
- Dee D P, Uppala S M, Simmons A J, Berrisford P, Poli P, Kobayashi S, Andrae U, Balmaseda M A, Balsamo G, Bauer P, Bechtold P, Beljaars A C M, Van De Berg L, Bidlot J, Bormann N, Delsol C, Dragani R, Fuentes M, Geer A J, Haimberger L, Healy S B, Hersbach H, Hólm E V, Isaksen L, Kållberg P, Köhler M, Matricardi M, McNally A P, Monge-Sanz B M, Morcrette J J, Park B K, Peubey C, De Rosnay P, Tavolato C, Thépaut J N and Vitart F (2011) The ERA-Interim reanalysis: configuration and performance of the data assimilation system *Quarterly Journal of the Royal Meteorological Society*. 137 656 553-597
- Dudhia J. (2014) A History of Mesoscale Model Development. *Asia-Pacific Journal of Atmospheric Sciences* 50 121-131. <http://dx.doi.org/10.1007/s13143-014-0031-8>
- Engel C B, Lane T P, Reeder M J and Rezny M (2013) The meteorology of Black Saturday *Quarterly Journal of the Royal Meteorological Society*. 139 672 585-599
- Evans J P, Ekström M and Ji F (2012) Evaluating the performance of a WRF physics ensemble over South-East Australia *Climate Dynamics*. 39 6 1241-1258
- Field C B, Barros V R, Mach K and Mastrandrea M (2014) Climate change 2014: impacts, adaptation, and vulnerability. Working Group II Contribution to the IPCC 5th Assessment Report—Technical Summary, 76 pp
- Georgescu M (2015) Challenges Associated with Adaptation to Future Urban Expansion *Journal of Climate*. 28 7 2544-2563
- Georgescu M, Morefield P E, Bierwagen B G and Weaver C P (2014) Urban adaptation can roll back warming of emerging megapolitan regions *Proceedings of the National Academy of Sciences*. 111 8 2909-2914
- Grell G A and Dévényi D (2002) A generalized approach to parameterizing convection combining ensemble and data assimilation techniques *Geophysical Research Letters*. 29 14 38-1-38-4
- Guan H, Soebarto V, Bennett J, Clay R, Andrew R, Guo R, Gharib S and Bellette K (2014) Response of office building electricity consumption to urban weather in Adelaide, South Australia *Urban Climate* 1 pp. 42-55
- Iacono M J, Delamere J S, Mlawer E J, Shephard M W, Clough S A and Collins W D (2008) Radiative forcing by long-lived greenhouse gases: Calculations with the AER

- radiative transfer models *Journal of Geophysical Research: Atmospheres*. 113 D13 n/a-n/a
- Imran H M, Kala J, Ng A W M and Muthukumar S (2017) An evaluation of the performance of a WRF multi-physics ensemble for heatwave events over the city of Melbourne in southeast Australia *Climate Dynamics*, in press. DOI <https://doi.org/10.1007/s00382-017-3758-y>
- Irvine P J, Ridgwell A and Lunt D J (2011) Climatic effects of surface albedo geoengineering *Journal of Geophysical Research: Atmospheres*. 116 D24 n/a-n/a
- Jackson T L, Feddema J J, Oleson K W, Bonan G B and Bauer J T (2010) Parameterization of Urban Characteristics for Global Climate Modeling *Annals of the Association of American Geographers*. 100 4 848-865
- Janjić Z I (1994) The Step-Mountain Eta Coordinate Model: Further Developments of the Convection, Viscous Sublayer, and Turbulence Closure Schemes *Monthly Weather Review*. 122 5 927-945
- Johansson E (2006) Influence of urban geometry on outdoor thermal comfort in a hot dry climate: A study in Fez, Morocco *Building and Environment*. 41 10 1326-1338
- Kala J, Andrys J, Lyons T J, Foster I J and Evans B J (2015) Sensitivity of WRF to driving data and physics options on a seasonal time-scale for the southwest of Western Australia *Climate Dynamics*. 44 3 633-659
- Kala J, Evans J P and Pitman A J (2015) Influence of antecedent soil moisture conditions on the synoptic meteorology of the Black Saturday bushfire event in southeast Australia. *Quarterly Journal of the Royal Meteorological Society*. 141 3118–3129. [doi:10.1002/qj.2596](https://doi.org/10.1002/qj.2596)
- Kusaka H and Kimura F (2004) Thermal Effects of Urban Canyon Structure on the Nocturnal Heat Island: Numerical Experiment Using a Mesoscale Model Coupled with an Urban Canopy Model *Journal of Applied Meteorology*. 43 12 1899-1910
- Kusaka H, Kondo H, Kikegawa Y and Kimura F (2001) A Simple Single-Layer Urban Canopy Model For Atmospheric Models: Comparison With Multi-Layer And Slab Models *Boundary-Layer Meteorology*. 101 3 329-358
- Li D and Bou-Zeid E (2014) Quality and sensitivity of high-resolution numerical simulation of urban heat islands *Environmental Research Letters*. 9 5 055001
- Li D, Bou-Zeid E and Oppenheimer M (2014) The effectiveness of cool and green roofs as urban heat island mitigation strategies *Environmental Research Letters*. 9 5 055002
- Li D, Bou-Zeid E, Barlage M, Chen F, Smith J A (2013) Development and evaluation of a mosaic approach in the WRF-Noah Framework *Journal of Geophysical Research: Atmospheres*. 118 11 918-11, 935, doi:10.1002/2013JD020657
- Liu Y, Chen F, Warner T and Basara J (2006) Verification of a Mesoscale Data-Assimilation and Forecasting System for the Oklahoma City Area during the Joint Urban 2003 Field Project *Journal of Applied Meteorology and Climatology*. 45 7 912-929
- Matzarakis A, Rutz F and Mayer H (2010) Modelling radiation fluxes in simple and complex environments: basics of the RayMan model *International Journal of Biometeorology*. 54 2 131-139
- Miao S, Chen F, Lemone M A, Tewari M, Li Q and Wang Y (2009) An Observational and Modeling Study of Characteristics of Urban Heat Island and Boundary Layer Structures in Beijing *Journal of Applied Meteorology and Climatology*. 48 3 484-501
- Millstein D and Menon S (2011) Regional climate consequences of large-scale cool roof and photovoltaic array deployment *Environmental Research Letters*. 6 3 034001
- Morini E, Touchaei A G, Rossi F, Cotana F and Akbari H (2017) Evaluation of albedo enhancement to mitigate impacts of urban heat island in Rome (Italy) using WRF meteorological model *Urban Climate* (in press)

- Morini E, Touchaei A G, Castellani B, Rossi F and Cotana F (2016) The Impact of Albedo Increase to Mitigate the Urban Heat Island in Terni (Italy) Using the WRF Model *Sustainability* 8 p. 999
- Nairn J and Fawcett R (2013) Defining heatwaves: heatwave defined as a heat impact event servicing all community and business sectors in Australia *The Centre for Australian Weather and Climate Research*. http://www.cawcr.gov.au/technical-reports/CTR_060.pdf. Accessed 22 Nov 2016
- Nicholls N and Larsen S (2011) Impact of drought on temperature extremes in Melbourne, Australia *Australian Meteorological & Oceanographic Journal*. 61 2 113 - 116
- O'malley C, Piroozfarb P a E, Farr E R P and Gates J (2014) An Investigation into Minimizing Urban Heat Island (UHI) Effects: A UK Perspective *Energy Procedia*. 62 Supplement C 72-80
- Oleson K W, Bonan G B and Feddema J (2010) Effects of white roofs on urban temperature in a global climate model *Geophysical Research Letters*. 37 3 n/a-n/a
- Perkins-Kirkpatrick S E, White C J, Alexander L V, Argüeso D, Boschat G, Cowan T, Evans J P, Ekström M, Oliver E C J, Phatak A, Purich A (2016) Natural hazards in Australia: heatwaves *Climatic Change*. 1–14. doi:10.1007/s10584-016-1650-0
- Rosenfeld A H, Akbari H, Romm J J and Pomerantz M 1998 Cool communities: strategies for heat island mitigation and smog reduction *Energy and Buildings*. 28 1 51-62
- Perkins S E and Alexander LV (2013) On the measurement of heat waves *Journal of Climate* 26 4500–4517
- Razzaghmanesha M and Razzaghmanesha M (2017) Thermal performance investigation of a living wall in a dry climate of Australia *Building and Environment* 112 45-62
- Razzaghmanesha M, Beechama S and Salemi T (2016) The role of green roofs in mitigating Urban Heat Island effects in themetropolitan area of Adelaide, South Australia *Urban Forestry & Urban Greening* 15 89–102
- Sharma A, Conry P, Fernando H J S, Alan F H, Hellmann J J and Chen F (2016) Green and cool roofs to mitigate urban heat island effects in the Chicago metropolitan area: evaluation with a regional climate model *Environmental Research Letters*. 11 6 064004
- Sharma A, Fernando H J, Hellmann J and Chen F (2014) Sensitivity of WRF model to urban parameterizations, with applications to Chicago metropolitan urban heat island *ASME 2014 4th Joint US-European Fluids Engineering Division Summer Meeting 14 Environ. Res. Lett.* 11 (2016) 064004 (American Society of Mechanical Engineers) p V01DT28A002
- Skamarock W C, Klemp J B, Dudhia J, Gill D O, Barker D M, Wang W and Power J G (2005) A description of the advanced research WRF version 2. NCAR technical note, NCAR/TND468 + STR. National Center for Atmospheric Research, Boulder
- Skamarock W C, Klemp J B, Dudhia J, Gill D O, Barker D M, Duda M G, Huang X-Y, Wang W and Powers J G (2008) A description of the advanced research WRF version 3. NCAR technical note NCAR/TN-475 + STR, National Center for Atmospheric Research, Boulder
- Smith K R and Roebber P J (2011) Green Roof Mitigation Potential for a Proxy Future Climate Scenario in Chicago, Illinois *Journal of Applied Meteorology and Climatology*. 50 3 507-522
- Song J and Wang Z-H (2015) Interfacing the Urban Land–Atmosphere System Through Coupled Urban Canopy and Atmospheric Models *Boundary-Layer Meteorology*. 154 3 427-448

- Steffen W, Lesley H and Sarah P (2014) Heatwaves: Hotter, Longer, More Often - Climate Council.
<https://www.climatecouncil.org.au/uploads/9901f6614a2cac7b2b888f55b4dff9cc.pdf>
- Sun T, Bou-Zeid E and Ni G-H (2014) To irrigate or not to irrigate: Analysis of green roof performance via a vertically-resolved hygrothermal model *Building and Environment*. 73 Supplement C 127-137
- Sun T, Bou-Zeid E, Wang Z-H, Zerba E and Ni G-H (2013) Hydrometeorological determinants of green roof performance via a vertically-resolved model for heat and water transport *Building and Environment*. 60 Supplement C 211-224
- Synnefa A, Dandou A, Santamouris M, Tombrou M and Soulakellis N(2008) On the Use of Cool Materials as a Heat Island Mitigation Strategy *Journal of Applied Meteorology and Climatology*. 47 11 2846-2856
- Taha H (2008a) Episodic Performance and Sensitivity of the Urbanized MM5 (uMM5) to Perturbations in Surface Properties in Houston Texas *Boundary-Layer Meteorology*. 127 2 193-218
- Taha H (2008b) Meso-urban meteorological and photochemical modeling of heat island mitigation *Atmospheric Environment*. 42 38 8795-8809
- Thompson G, Field P R, Rasmussen R M and Hall W D (2008) Explicit Forecasts of Winter Precipitation Using an Improved Bulk Microphysics Scheme. Part II: Implementation of a New Snow Parameterization *Monthly Weather Review*. 136 12 5095-5115
- Touchaei A G, Akbari H and Tessum C W (2016) Effect of increasing urban albedo on meteorology and air quality of Montreal (Canada) - Episodic simulation of heat wave in 2005 *Atmospheric Environment*. 132 188-206
- Vatani J, Golbabaie F, Dehghan S F and Yousefi A (2016) Applicability of Universal Thermal Climate Index (UTCI) in occupational heat stress assessment: a case study in brick industries *Industrial Health*. 54 1 14-19
- Victorian Auditor General's Report (2014) Heatwave Management: Reducing the Risk to Public Health.
<http://www.audit.vic.gov.au/publications/20141014-Heatwave-Management/20141014-Heatwave-Management.pdf>
- Wong N H, Cheong D K W, Yan H, Soh J, Ong C L and Sia A (2003) The effects of rooftop garden on energy consumption of a commercial building in Singapore *Energy and Buildings*. 35 4 353-364
- Yang J, Wang Z-H, Chen F, Miao S, Tewari M, Voogt J A and Myint S (2015) Enhancing Hydrologic Modelling in the Coupled Weather Research and Forecasting–Urban Modelling System *Boundary-Layer Meteorology*. 155 1 87-109